NIPER-729
Distribution Category UC-122
December 1993

Topical Report

PETROPHYSICAL CHARACTERISTICS ASSOCIATED WITH BOUNDING SURFACES IN ALMOND FORMATION COREHOLE NO. 2, SWEETWATER COUNTY, WYOMING

Project SGP69, milestone 6, FY93

by Richard Schatzinger, Michael Szpakiewicz, Bijon Sharma and Susan Jackson

Work Performed for
U. S. department of Energy
Under Cooperative Agreement DE-FC22-83FE60149

Bartlesville Project Office
U.S. Department of Energy

IIT Research Institute
National Institute for Petroleum and Energy Research
P. O. Box 2128
Bartlesville, Oklahoma 74005
(918) 336-2400

TABLE OF CONTENTS

TABLES

TABLE OF CONTENTS (continued)

Page

ILLUSTRATIONS

PETROPHYSICAL CHARACTERISTICS ASSOCIATED WITH BOUNDING SURFACES IN ALMOND FORMATION COREHOLE NO. 2, SWEETWATER COUNTY, WYOMING.

by Richard Schatzinger, Michael Szpakiewicz, Bijon Sharma and Susan Jackson

ABSTRACT

The objectives of this work are to characterize the fluid flow properties of bounding surfaces of genetic sandstone units in the Almond Formation. This report covers the initial stages of characterizing and measuring the petrophysical properties of one bounding surface. Corehole no. 2, located approximately 0.5 mi downdip from outcrop exposures of the Almond Formation, was selected for study because the bounding surfaces are well preserved, and yet it is close to outcrop exposures so that the dimensions of the units and surfaces can be determined.

Petrographic analyses and mercury porosimetry measurements were conducted on eight samples. X-ray diffraction (XRD) measurements of mineral composition were made in four of the eight samples. The average sandstone framework composition of the eight samples is 56.5% quartz, 15.4% feldspar, and 27.9% rock fragments. Flood tidal delta sands are texturally more mature, but mineralogically and lithologically less mature than tidal channel sands. This may be due to different rates of deposition and different energies in the environment of deposition.

Thin section point counts indicate generally low porosities ranging from 3.0 to 15.1%, most probably due to the compacted nature of the sandstones, the tight packing indices and the relatively great amounts of total cement. Pore throat sizes are relatively small, with median throat radii ranging from 1.7 to 8.0 microns. Compaction and cementation have tended to "disconnect" surviving pores, allowing communication only through small throats.

The sequence of diagenetic events can be summarized (early to late): quartz overgrowths, calcite cement and replacement, fine dolomite cementation and replacement, cementation and replacement by pyrite, cementation and replacement by kaolinite, dissolution of unstable grains, cementation and replacement by medium crystalline euhedral dolomite, and compaction and grain fracture. These stages are overlapping, and chemical compaction was masked by precipitation of dolomite, pyrite and sometimes kaolinite cements.

Geochemical analysis of the vadose and phreatic zones of the groundwater table in the Rock Springs Uplift area were undertaken to assist in the identification of the timing of diagenetic features observed in Corehole no. 2 and associated outcrops, and to assist in determining those diagenetic features that may be comparable to the subsurface. In the area around Corehole no. 2, ground waters flow generally southeast with a hydraulic gradient of 133 and 166 ft/mi. Depth to the water table ranges from 25 ft in topographically low areas, to more than 500 ft in high areas.

Ground waters in the Upper Almond infiltrate the Rock Springs Uplift and gain their chemical composition while flowing downdip (but up stratigraphic section) through the Rock Springs, Erickson, and lower Almond formations. The approximate subsurface residence time for water molecules in 1.5 to 2.0 million years. In the shallow geochemical zone of Corehole no. 2, the mineral mass transport primarily results from the breakdown of carbonates, silicates, and sulfides. Hydrolysis of the carbonates causes mobilization of metals and an increase in alkalinity and amounts of bicarbonate in solution. Silicates including orthoclase are transformed to kaolinite.

ACKNOWLEDGMENTS

Jerry Easter of Oxy USA, Inc., Tulsa, Oklahoma provided the core. Sam Swan performed the mercury porosimetry measurements; Robert Schaffitzel and Dwight Haney conducted the CT and minipermeameter measurements. Technical reviews were provided by Mike Madden, Min Tham and Edith Allison. Viola Rawn-Schatzinger provided editorial assistance, Djaun Grissom provided computer graphics and Edna Hatcher performed the word processing.

INTRODUCTION

The permeability and porosity characteristics within sedimentological units have been addressed in recent studies; however, the fluid flow characteristics of the bounding surfaces separating sedimentological units are not well known. Knowledge of the flow characteristics of these surfaces (e.g., bedding planes, facies contacts, flooding surfaces) is essential for the delineation of flow units in reservoir model construction. The objective of this work is to characterize the fluid flow properties of bounding surfaces of genetic sandstone units in the Almond Formation. This report covers the initial stages of this investigation within an ongoing study of the Almond Formation in Patrick Draw field and outcrop exposures around the Rock Springs Uplift (Figure 1).

Core from Corehole no. 2, located ~0.5 miles downdip of Almond Formation outcrop exposures, Sweetwater county, WY, was used for this part of the study. Figure 2 shows the location of Corehole no. 2 and outcrops RG and RH, previously described (Jackson and Rawn-Schatzinger, 1993).

Corehole no. 2 was selected for study because it is near the outcrops and the contacts (bounding surfaces) between units are more easily sampled than the typically weathered contacts of the outcrop. Information from the nearby outcrop exposures will be used to establish the stratigraphic framework and architectural unit hierarchy of depositional units, as well as the geometry and dimensions of the surfaces. The outcrops provide an important source of information because the interpretation of depositional processes from vertical profiles is difficult. Miall (1986) correctly asserts that vertical profiles cannot adequately discriminate complex three-dimensional systems of channelized environments, nor can they readily distinguish tectonic from autocyclic effects such as shifting of a channel.

Corehole no. 2 was described, interpreted and minipermeameter and Computed Tomography (CT) density measurements were made. Petrographic analyses and mercury porosimetry measurements were conducted in eight samples. X-ray diffraction (XRD) measurements of mineral composition were made in four samples. In addition, information on the groundwater flow and geochemistry has been collected to assist in identification of the timing of diagenetic features observed in thin sections. Information from electrical, Spontaneous Potential (SP), gamma ray and density logs from Corehole no. 2 were integrated with the analyses of CT density and minipermeameter and grain size measurements to determine the variations in petrophysical properties at different scales.

Subsequent field work will address the regional stratigraphic framework and better definition of the three-dimensional facies architecture of the complex tidal deposits of the Upper Almond Formation. Geologic data from corresponding outcrop exposures will not only assist in the interpretations of the outcrop core, but will provide the basis for subsequent work to determine the dimensions and geometries of the bounding surfaces once the flow characteristics of the bounding surfaces have been determined. The bounding surfaces have typical geometric shapes, areal extents and lithofacies associations and can be used to define hierarchies of depositional units or architectural elements. This information could then be used to better understand the architecture and, therefore, the production characteristics of reservoirs producing from the Almond such as Patrick Draw and Table Rock fields

Mercury Porosimetry Measurement

Mercury porosimetry data were obtained utilizing the Quantachrome-AUTOSCAN-60. Sample size, usually 2-6 grams, is limited by the volume of the penetrometer (figure 3) and the porosity of the sample. The filling apparatus serves to evacuate the sample, fill the penetrometer with mercury and obtain data from near vacuum to ambient conditions. The sample is then moved to the AUTOSCAN-60 for the high pressure phase of the experiment. The penetrometer has a wide base with a ground glass lip at the bottom, a stem of precision bore tubing with regard to both the inside and outside diameters, and a length of curved standpipe extending into the base to prevent fine particles from floating into the stem when the cell is filled with mercury. A metal sheath around the stem and an electrode attached to the ground glass lip of the base provide the electrical contacts. Once the penetrometer is filled with mercury the capacitance is measured by the instrument. As the pressure is increased and the mercury is pushed into the sample the capacitance changes indicating the amount of mercury absorbed by the sample. A computer dedicated to the system reads the mercury volume and pressure at least seven times a second but stores only those values separated by defined pressure differences. The data collected during the low pressure run and the high pressure run are combined to form a continuous set of data points from near vacuum to the final high pressure data point. Approximately 600 data points are collected in a full intrusion scan. From this data the size of the pore throats controlling percentages of pore volume can be calculated using the following formula.

$$Pr = -2\gamma \cos \theta$$

Where P is the applied pressure, r is the pore radius, γ is the surface tension of mercury, and θ is the contact or wetting angle between mercury and the surface.

Core Description

A description of the interval 30-300 ft below ground level in Corehole no. 2 and preliminary facies interpretation is presented in figure 4. The described interval begins with back barrier and tidal-inlet related deposits of a coal (Waxwing coal of Roehler, 1988) and an associated lagoonal deposit (300-291 ft) overlain by an oyster shell-bearing tidal channel fill. A transgressive flooding surface follows with a regressive sequence of shoreface (270-241 ft) overlain by tidal delta and backbarrier coal and lagoonal deposits. The interval of 291.6 to 274.7 ft, from the base of the coquina channel and the transition to marine shoreface deposits were selected for initial study and petrophysical measurements.

This interval contains two orders of architectural units A channel tentatively classified as group 7 and a flooding surface marking the end of a barrier sequence tentatively classified as group 8 (Table 1). Further delineation of the regional stratigraphy will be necessary to increase the confidence level in the group assignations. The classification presented in Table 1 groups architectural units into ten classes spanning at least twelve orders of magnitude of time scale (Miall, 1991). The grouping is based primarily on the total time elapsed during the formation of the deposit and its bounding surface.

PETROGRAPHIC ANALYSIS OF SAMPLES FROM ALMOND COREHOLE NO. 2

Methods

Eight representative thin sections were selected from intervals with identified depositional facies in Almond Corehole no. 2 (Table 2). Thin sections were stained for K-feldspar and calcite. Detrital and authigenic composition as well as porosity were determined by standard optical examination including point counts consisting of at least 250 points per thin section. In addition, four rock samples were analyzed by X-ray diffraction (XRD) in order to confirm the petrographic results and identify minerals that might not be easily differentiated or identified by optical methods, particularly clay types. In order to determine the distribution of pore throat radii, mercury porosimetry was performed on duplicate samples cut from the original thin section plugs.

Texture

The Almond samples studied consist of fine sandstone and silty sandstone. The sandstones contain less than 2% detrital clay matrix and are classified as "clean." The tidal channel and channel fill sandstones are dominantly subangular and moderately sorted resulting in a textural maturity classification of submature. Flood tidal delta samples, in contrast tend to be subrounded and well sorted resulting in a texturally mature classification.

Framework Grain Composition

Almond sandstones in Corehole no.2 are litharenites to sublitharenites with an average composition of 56.5% quartz, 15.4% feldspar, and 27.9% rock fragments ($Q_{56.5}F_{15.4}R_{27.79}$ (figure 5, Table 2). Proportions of framework grain types are relatively constant. Detrital quartz constitutes from 28.8 to 57.0% of the total rock volume; however, it ranges between 51.8 and 68.9% of the essential constituents (quartz, feldspar, and rock fragments). Feldspars are almost exclusively the K-feldspar variety. They range from 4.5-13.1% of the total rock volume, and 9.6-20.1% of the essential constituents.

More than half of the feldspars have been altered or leached to some extent. Although these values were not tabulated during the point counting, much more than half of the changes noticed in K-feldspars were due to alteration to clay, probably kaolinite, and replacement by dolomite. Sericitization was also noted. Although increase in total porosity by leaching of feldspars is common, the amount of secondary porosity created is not volumetrically significant. Thus, the feldspar content may have been only a few percent greater in the original sandstone. An exception is sample, 282.3 (Table 3) that contains more than 30% total rock volume dolomite which is highly replacive of detrital minerals, especially feldspars.

Sedimentary rock fragments including chert, shale, and silty shale are the most common lithic grains. A few glauconite grains were noted in the sample from 282.2 ft, and that from 274.7 ft contains 4.5% glauconite. This much glauconite suggests that the depositional environment at 274.7 ft is more marine than the "abandoned channel fill" listed in Table 2. A shoreface environment may be more likely. Metamorphic and highly altered or compacted volcanic rock fragments also comprise a small percent of the lithics fraction, but were not tabulated separately in the point count data. Lithics range from 9.4-24.4% total rock volume and comprise 21.0-36.3% with an average of 27.9 of the essential constituents. Most of the lithics including clay-rich rock fragments, metamorphic and volcanic rock fragments, and glauconite are ductile, frequently being highly compacted between quartz, feldspar, and chert grains. Although sand sized muscovite mica is rare in the samples examined it also is very ductile and easily compressed between other framework grains.

Two of the three flood tidal delta samples are litharenites (three times as many lithic fragments as feldspars) while all of the tidal channel samples are feldspathic litharenites (Fig. 5). This relationship is perplexing because the more texturally mature samples from the flood tidal delta are generally mineralogically and lithologically less mature (contain greater amounts of the highly unstable lithic fragments). On the other hand the less texturally mature sandstones from the tidal channel facies are more mineralogically and lithologically mature in the sense that they contain less of the unstable lithic fragments. Perhaps more of the lithics in the tidal channel sandstones, which are dominantly clay-rich sedimentary rock fragments, were very rapidly destroyed by the high energy environment of deposition. During the same relatively short period of time the other dominant terrigenous grains (quartz and feldspars) were less susceptible to physical degradation. Therefore, even though the tidal delta sandstones are better

sorted and contain a more rounded terrigenous grain fraction, the depositional energy was less, resulting in a higher sedimentation rate and less destruction of sedimentary rock fragments.

Oyster shells or fragments of shells were present in tidal channel and the underlying flood tidal delta facies. Visual examination of the core shows that oysters are not evenly distributed through the tidal channel and tidal delta facies, but rather are very abundant in thin, discontinuous zones. Oysters were conspicuously absent from the transitional upper portion of the tidal channel between 280.5-282.5 ft. Thin section analysis indicates that the oyster shells were strongly leached along growth lamellae and provide an abundant local source for calcite cement.

Cements And Replacive Minerals

Cements and replacive minerals constitute between 16.3 and 40.0% of the sandstone volume in the Almond Formation samples from Corehole no. 2 that were examined petrographically. The average volume of cement and replacive minerals in the sandstones is 24.2%, exclusive of the very fine alteration material, probably kaolinite, seen in feldspars. This high a value seems somewhat incongruous considering the rather friable nature of the sands when pieces are crushed between the fingers. However, most of the effective cement is poorly interlocked very-fine to fine-grained anhedral dolomite, based on optical examination, that does not add significant consolidation to the rock. Less abundant cements are clay cement, medium-crystalline growth banded euhedral dolomite, calcite, quartz overgrowths, siderite, and pyrite.

Dolomite cements include both very-fine grain to fine grain, anhedral crystals that are also somewhat replacive. Fine-grained dolomite is present in all sandstones examined. Based on the few samples available it appears that there is no consistent relationship between fine dolomite and depth. Fine dolomite most occurrences the fine dolomite is concentrated around the margins of primary pores indicating its dominant cement origin. Fine dolomite is also found within framework grains and clearly replaces margins of any other mineral. Locally massive amounts of fine dolomite still retain ghosts of previous grains that are nearly completely replaced. Fine dolomite ranges from 4.5-30.4% with an average of 13.3%. Trace amounts of siderite were intermixed with the fine dolomite and tentatively identified optically.

Another type of dolomite cement is medium- to coarsely-crystalline growth-banded euhedral cement. It is very distinctive in the tidal channel facies where, based on the samples analyzed petrographically, there is an increasing-upward amount from 290.5-282.2 ft. The coarser, euhedral dolomite is present but rare in the underlying tidal delta facies. This type of dolomite has a volume of between 0.0 and 6.9%, with an average of 3.1% in the tidal channel facies and an average of 0.9% in the tidal delta facies.

Based on petrographical analysis, calcite cement is only present at more than trace levels in the sample from 290.5 ft. Here it comprises massive medium- to coarse-crystalline, anhedral to subhedral cement and grain-marginal replacements. Pores in this thin section are very poorly connected because of the pervasive interparticle calcite cement. In this sample, oysters have been strongly leached along shell growth lamellae creating very complex partially moldic porosity within the oyster shells. Preserved microboring in the oysters has been filled with pyrite cement. In addition, pyrite cement is present as micron-size framboids. More massive pyrite also filled pore space, and partially replaced nearby grains around the exterior of the now-leached oyster shells. In the sample from 290.5 ft there is 6.4% total pyrite cement. Elsewhere, total pyrite cement comprises trace amounts to 1.2% of the rock based on point counts.

Quartz overgrowths vary between rounded inherited cements on reworked detrital quartz grains to pore-reducing euhedral overgrowths more than 100μ. Many of the quartz overgrowths are easily distinguished from the host grains by a thin "dust trail" along the contact between cement and detrital grain. Differences in inclusion densities along the margins of other quartz grains may, however, indicate less obvious quartz overgrowths. None of the overgrowths were included in the point counts, but their abundance probably ranges up to 5% or more in the thin sections examined. Because of the importance of quartz overgrowths with respect to rock strength and resistance to compaction, further efforts should be undertaken to accurately determine the amount of quartz cement and define more clearly its place in the paragenetic sequence. Cathodoluminescence may provide an easy method to improve the estimates of quartz overgrowths.

XRD Analysis

Companion samples from four of the thin sections were analyzed by XRD. The results are presented in Table 4. These results are very disappointing when compared to the mineralogy determined by petrography. It will be noticed immediately that the amount of quartz in the XRD results is nearly twice that determined by optical methods. The XRD-derived dolomite and total clay content are completely unlike their optically-determined counterparts. Even taking into consideration the differences inherent in the two methods, there seems to be, at this time, no way to reconcile the two data sets. Further work will be necessary to check and re-run the XRD samples.

Pore Space

Interparticle porosity is approximately five times more abundant than intraparticle or moldic porosity. Based on thin section point counts, porosity varies between 3.0-15.1%, however, there is petrographical evidence that the higher values may have been created by faulty sample preparation. Discounting the suspected samples, porosity is no greater than 8.8% in these sandstones. Microporosity, especially within and between pore-reducing kaolinite, and in degraded minerals such as feldspar, and within cherts is impossible to properly assess in thin section and can significantly alter results. Therefore, thin section porosity should only be taken as an indicator of total porosity.

Intraparticle porosity in K-feldspars that had been partially leached is present in the samples but not as important as that from the Almond Formation at Patrick Draw field. Due to compaction, fracture porosity is common where grains have been cracked and separated due to the stress of physical and chemical compaction. Porous fractures in brittle grains such as K-feldspars is common, but not volumetrically important. Based on the amount of physical and chemical compaction evident in the types of grain contacts, the amount of porosity gained by leaching and fracturing is far less than that lost to compaction.

In samples with abundant amounts of finely-crystalline anhedral dolomite, fine intercrystalline porosity may be significant. Scanning electron microscopy (SEM) of samples could help to define the relative abundances of reduced primary, intercrystalline, and microporosity. Where matrix and dolomite cement is minimal, pores are commonly reduced by microporous kaolinite cement. Thus, because of the amount of compaction, degree of cementation, and probable importance of microporosity, the functional porosity (that porosity through which fluids may be expected to flow in significant quantity) is, in general, quite reduced in these sandstones.

Based on the amount of cement and compaction observed during petrographical analysis one would predict that the pore throats in these samples would be quite small. To test this hypothesis companion samples from all the thin sections were subjected to mercury injection porosimetry. The results indicate that the median throat radius for the entire sample suite is remarkably similar (Table 3) and small, ranging from 1.7 to 8.0μ with an average of 2.8μ. The sample with the greatest median throat radius (8.0μ) is the tidal channel sandstone with oysters leached along the shell growth lamellae. This creates highly elongate pores within the confines of the original shell and poorly sorted pore throats where breaks between the lamellae exist. Based on the mercury-injection curves in figure 6, sorting of pore throats is very similar for seven of the eight samples. The stratigraphically highest sample (274.7 ft) has the most uniform throat size sorting and that from 290.5 ft is slightly different from the others, having clearly the least uniform throat size sorting.

The generally compacted nature of the sandstones as seen in thin sections, and their relatively great amount of total cement (average 24.2%) can explain their low porosity. Compaction and cementation also tend to "disconnect" the remaining pores and allow communication only through small throats as can be shown in the mercury-injection curves in figure 6.

Diagenetic History

The paragenetic sequence for diagenetic phases from the eight sandstone samples was determined from petrographic relationships. Major differences in diagenetic history could not be deduced from the small number of samples available. Therefore, petrographic observations were accumulated from all of the thin section samples to derive the overall sequence of diagenetic stages. Eight major stages were recognized and their relative timing was determined (Fig. 7). The diagenetic phases identified include 1) precipitation of quartz overgrowths, 2) cementation/replacement by medium to coarse crystalline calcite, 3) cementation/replacement by fine dolomite, 4) cementation/replacement by pyrite, 5) cementation/replacement by kaolinite, 6) a phase of dissolution of unstable grains and fossils, 7) cementation/replacement by coarse-grained euhedral dolomite, and 8) compaction and grain fracture. Although physical compaction begins at the time of deposition, strong chemical compaction (solution-reprecipitation processes) was not very noticeable until after the precipitation of fine dolomite, pyrite, and some kaolinite cements.

No other diagenetic precipitate was found to predate quartz overgrowths. Quartz overgrowths, however, clearly predate the other very early cement, calcite. Medium to coarse crystalline calcite is a very early cement. It has stopped compaction in highly cemented samples so that anomalously high numbers of "floating" terrigenous grains are preserved. In a point count of the sample from 282.3 ft with 29.1% calcite cement, 22% of the grains had no contacts with surrounding sand grains. While this is far less than the 87.5% and 79.5% of grains with no contacts in unconsolidated fluvial and beach sands respectively (Wilson and McBride, 1988), it is high for a clean (no clay matrix) lithified sandstone. The high percent of floating grains in the calcite-cemented Almond sandstone at 282.3 ft indicates that the cement precipitated very soon after deposition, or at least well before significant burial and subsidence. The mass balance between calcite cement and the amount of oysters (or their moldic remains) in the

sandstones is strongly in favor of calcite cement. The high amount of calcite cement (more than 29% in the sample from 282.3 ft) could have been provided by the volume of oysters (3%), and so, at least on the scale of a thin section, the system must have been open at this time with a net influx of $CaCO_3$. There is additional evidence that leaching of the oysters postdated precipitation of calcite cement. Cross cutting and pore filling relationships indicate that pyrite cement post dates calcite cement. Pyrite fills microborings in preserved parts of the oyster shells and pyrite cement forms the pore filling around oysters that are now moldic. Thus, if calcite cement predates pyrite cement, and pyrite preceded leaching of the oysters, then calcite cement must have precipitated prior to leaching of the oysters. The occurrence of pyrite at this point in the paragenetic sequence, distinctly prior to leaching of unstable grains, indicates that the sediments must have rather quickly become reducing rather than oxidative. There is very little iron oxide surrounding the massive pyrite cements or the very fine grained framboidal pyrite. Framboidal pyrite, such as is common in the calcite-cemented sample (5.6%), is often taken to have originated by microbial association in a reducing microenvironment.

Pyrite is "fresh" in thin section and very little iron oxides are present as auras around the pyrite. Pyrite also clearly predated leaching. These relationships provide a line of evidence that the subsequent leaching of oysters, feldspars, and some lithics may have also been due to corrosive anaerobic waters. This "conclusion" is rather weak, however, because of the small number of samples examined. Certainly many more samples need to be analyzed to validate these observations.

The most volumetrically significant pore filling is finely crystalline dolomite (Table 3). Despite fine dolomite being important in all other samples, it comprises only 4% of the strongly calcite cemented sample. This can be interperted that nearly all of the fine dolomite precipitated after calcite. Fine dolomite tends to occur around the margins of pores whose remainder has been filled with kaolinite cement indicating that most kaolinite post dates the fine dolomite. Kaolinite is, however, dominantly a post compaction pore filling. It also occurs as a degradation product in altered K-feldspars.

At this time only a single stage of leaching can definitely be identified in the thin sections. Based on petrographical relationships the leaching event is only post dated by most medium to coarse crystalline euhedral dolomite cement, some kaolinite cementation, and the later stages of compaction including grain fracture.

In order to investigate the effect of compaction, packing parameters were measured on 200 grains for each of four thin sections (Table 3). The following types of grain contacts were identified in thin section: floating (no contacts); tangential (or point); long; concavo-convex (embayed); and sutured (or serrated). From these observations, the contact index (CI) (Pettijohn, et al. 1972), which is the average number of contacts per grain, and the tight packing index (TPI) (Wilson and McBride, 1988), the average of long, concavo-convex, and sutured contacts per grain, were calculated.

The four samples whose packing indices were determined occur in less than 1.5 ft vertically and can, therefore, be considered essentially at the same stratigraphic horizon. CI ranged from only 1.49 to 3.40 while the TPI varied from as low as 0.39 (abundant early calcite cement in sample and a total cement content of 40%) to 3.96 (sample with no calcite cement and a total cement content of only 16%). These data indicate that for samples from essentially the same horizon, significant differences in packing (i.e., compaction) exist and may be related to amount and timing of cementation. Compaction can be demonstrated to strongly affect petrophysical properties of reservoir sandstones (Housknecht, 1984). Further research into this topic, particularly along well defined contacts in outcrop could shed light on lateral variations in compaction, that have been virtually ignored in the literature.

Although the data set is very small (eight thin sections analyzed), relationships between diagenetic and lithological features recorded in table 3 were examined. The only statistically significant relationship ($R = 0.97$) was a negative one between grain size and bulk quartz content. This indicates that the coarser-grained sands are more mineralogically immature. The finest sands examined in this study were right at the coarse silt-very fine sand grain size boundary. In addition, silts tend to be inherently enriched in the most stable grains such as quartz and so the observed relationship between grain size and quartz content is intuitively acceptable.

Significantly, no relationships were found between currently available diagenetic or lithological properties and depth or petrographically determined clay content. Certainly the analysis of additional samples for features such as permeability and laboratory-derived porosity would makes such conclusions more acceptable. Further, because only four samples were analyzed for packing (TPI or CI), it is believed that no statistically significant relationships can be determined between these features and the remainder of the petrographical data in table 3.

Discussion

Representative thin sections were analyzed from Almond Corehole no. 2 between depths of 274.7-291.6 ft. The average sandstone composition of essential components for eight samples is 56.5% quartz, 15.4% feldspar, and 27.9% rock fragments which is well within the sublitharenite field of ternary classification diagrams of Folk (1968). Two of the three flood tidal delta samples are litharenite, while all of the tidal channel samples are feldspathic

litharenite. The more texturally mature samples from the flood tidal delta are generally mineralogically and lithologically less mature. This relationship may be due to different rates of deposition and different energies in the environment of deposition.

Because the data base is small, with only eight analyzed thin sections, no differences in diagenesis can be determined between facies. Additional work that would enlarge the data base may shed light on this problem. The data base is, however, large enough to identify the major diagenetic phases. Cements and replacive minerals constitute an average of 24.2% of the thin sections. The most common diagenetic cements include fine crystalline dolomite followed in abundance by clay cement (dominantly kaolinite). Additional cements, in order of decreasing abundance include medium to coarse crystalline euhedral dolomite, calcite, quartz overgrowths, siderite, and pyrite.

Interparticle pore space in the analyzed samples is approximately five times more abundant than intraparticle or moldic porosity. Thin section point counts indicate 3.0-15.1% porosity, although values above 10% may be due to thin section preparation techniques. Microporosity may be significant in samples with abundant fine crystalline dolomite and kaolinite cement. Because of this, the thin section porosities should only be used as a relative guide to the amount of total porosity. The generally compacted nature of the sandstones with high averages of contact indices and tight packing indices and the relatively great amount of total cement can explain their low porosities. Pore throat sizes determined by mercury-injection capillary pressure are also quite small, with median throat radii ranging from 1.7-8.0μ. Compaction and cementation have tended to "disconnect" surviving pores, allowing communication only through small throats.

The paragenetic sequence for the examined samples includes (from early to late): quartz overgrowths, calcite cement and replacement, fine dolomite cementation and replacement, cementation and replacement by pyrite, cementation and replacement by kaolinite, dissolution of unstable grains, cementation and replacement by medium crystalline euhedral dolomite, and compaction and grain fracture. The stages are overlapping. For example, although some kaolinite precipitation may have overlapped with the later stages of calcite precipitation, kaolinite is predominantly a post compaction phase. Also, strong chemical compaction noted in the thin sections was not very noticeable until after precipitation of fine dolomite, pyrite, and some of the early kaolinite cements.

PETROPHYSICAL PROPERTY VARIATIONS IN SEDIMENTARY UNITS AND BOUNDING SURFACES FROM CORRELATIONS OF WIRELINE LOG AND CORE DATA

Introduction

The objective of this analysis is to determine from the integration of different types of wireline log and core data, the distribution of petrophysical properties in the sedimentary units and bounding surfaces of a nearshore sandstone deposit that control fluid production from such a reservoir. Information obtained from interpretation of the electrical (induction and short normal), SP , gamma ray and density logs from Corehole no. 2 were integrated with the analyses of CT density, minipermeameter and grain size measurements to determine the variations in petrophysical properties at different scales. The role of different sedimentary and diagenetic features in the facies of a nearshore sandstone deposit in controlling movement of fluid in the reservoir is investigated.

Wireline logs were digitized at 0.5 ft depth intervals for interpretation of the petrophysical properties. Variations in the petrophysical properties from sedimentological features thinner than 6", are beyond the resolution limit of the logging tool and may not be reflected on the log data. The logs give the average effect of a certain rock volume (around 2-3 cubic ft for the density log) and, therefore, the effect of a small sedimentary or diagenetic feature that may have a significant effect on fluid flow in the reservoir, may not always be resolved on these logs. Measurements of permeability with the minipermeameter are essentially a surface measurement that give rock permeabilities over a much smaller rock volume (of the order of 1-2 cubic centimeters for the average rock types). The CT density gives the bulk densities over about 50 cm^3 of the rock volume. The combined interpretations of wireline log and core data are expected to provide information on the effect of different scale depositional and diagenetic features in controlling the entrapment and movement of fluid in the reservoir. The binocular microscope and the comparator were used for a rapid estimation of the grain size variations for determining the degree of correlation between the grain size and the permeability distributions. The information obtained from interpretations of wireline log and core data were correlated with the geological descriptions of the sedimentary units and the facies in Corehole no. 2. A depth adjustment of 2 ft to the wireline log data was needed for matching the core and the log data.

Analysis Of Data

Petrophysical Property Variations in Bar 'F'

The petrophysical properties were computed for the entire length of the core in Corehole no. 2 but discussions here will be confined to the sandstone units in the lowermost bar deposit occurring at a depth of 182.8 ft and extending up to 295.5 ft. This bar has been referred to as bar 'F' in the earlier discussions. For ease of geological and petrophysical correlations, the three main sandstone units (identified as sand no. 1, 2 and 3) in bar 'F' have been studied individually. The distributions of clay content (V_{cl}) from analysis of gamma ray logs, porosity from analysis of gamma ray and density logs, permeability and grain size distributions from measurements with the minipermeameter and the microscope; respectively, were obtained from core samples from the three sandstones in bar 'F'. Except for porosity variations which will be discussed later, the distributions of the other petrophysical properties have been plotted in Figures 8a, 8b, 8c.

Earlier studies (Sharma, 1992) on the estimation of clay content in the Patrick Draw field from subsurface data, reported that the clay content from the log data was on an average about 3-4 percentage points higher than that obtained from XRD analysis. The presence of non-clay minerals like potassium feldspar or mica in the sandstones could contribute to excess gamma ray emissions that result in estimation of abnormally high clay values (Crain, 1986). If the XRD values are accepted as correct, then reasonably good estimation of clay distribution may be made by subtracting about 4 percentage points from the gamma-ray-derived values in order to eliminate the effect of non-clay radioactive minerals. A greater correction to the clay data, from Corehole no. 2, however, may be needed because of the large amounts of organic remnants found in the core which may further increase the gamma ray readings causing estimated clay values to be much higher than the actual. A comparison of gamma-ray-derived clay values with those obtained from XRD analysis or other sources will enable us to decide on the correction necessary to obtain the correct clay volumes. It should be mentioned that while the gamma-ray-derived values may not be very accurate, the clay profiles should provide information on the variation in clay content across the three sandstones.

The minipermeameter measured permeabilities across the three sandstones (Figs. 8a, 8b and 8c) indicate much sharper fluctuations compared to the V_{cl} values, this is because permeability varies over a large range within a

short vertical distance. A smooth curve drawn through the permeability values indicates that overall, the permeability variations in the three sandstones have an inverse relationship with variations in the clay content. The distribution of grain sizes indicates a moderate, positive correlation of grain size and permeability (r = 0.55 between grain size and logarithms of 3-point running average of minipermeability data) in the three sandstones. This moderate correlation between grain size and permeability was observed from studies of subsurface core data in the Bell Creek and the Patrick Draw fields (NIPER-700).

Correlation of Geological Features With Petrophysical Property Variations in Sand No. 1 (from 182 to 237 ft)

The permeability, clay content and the grain size variations in this tidal delta and swash bar deposit is shown in Figure 8a. The top, coaly part of the sandstone (from 182 ft to 185.5 ft) is easily distinguishable on logs by its low density and gamma ray values. The permeability in this zone should be close to zero. The clay content in the coaly zone is 0%, although the plotted value is shown to be slightly negative because the calculations were performed for a sandstone matrix. Immediately below the coaly zone is a rooted, laminated zone extending up to 189 ft where the clay content is moderately high. The permeability (not measured) in this zone is expected to be very low. Below the rooted structure is the cleanest part of the sandstone (from 189 to 200 ft) with high permeability (700 to 900 mD), low clay content (around 1-2 %), and large grain sizes (250-300 microns). The sandstone gets progressively cleaner upwards (Fig. 8a). The bottom of the sandstone shows laminations which are indicated on the mini permeability data by sharply varying permeability. Because of the averaging effect on logs, these laminations are not clearly reflected on the V_{cl} data.

Below the laminated zone, the clay content increases (averaging about 12%) and the permeability decreases (averaging about 250 mD) because of geological features such as clay clasts, burrows, etc. There are thin high permeability layers in this zone where the permeability increases up to 500 mD, and also low permeability zones of diagenetic aureoles around clay clasts where the permeability decreases to 50 mD or less. Below 232 ft the sandstone shows a sharp increase in clay content and decrease in permeability because of the increase in clay clasts.

In summary of the petrophysical properties of sand no. 1 the 3-fold enhancement of permeability in the top part of the sandstone compared to the bottom part may be attributed to clean sandstones with low clay content that are devoid of geological features that reduce permeability. The presence of diagenetic zones reduces the permeabilities to very low values. Because of the large permeability differential between the top and the bottom parts of this sandstone, a producing reservoir with a similar permeability profile is expected to behave like two or more separate reservoirs with widely different flow rates. Due to the laminations and the high and low permeability streaks, a good deal of fingering is expected in the flow profile of such a reservoir. The top, coaly, and the bottom, clayey zones of the reservoir have effectively zero permeabilities. The fairly uniform density values(around 2.1 gm/cm^3) from the bottom of the coaly zone at 189 ft to the top of the clayey zone at 232 ft indicate that this sandstone is devoid of significant amounts of heavy minerals like carbonates.

Sand No. 2 (from 238 to 265 ft)

The top part of this sandstone (from 237 to 241 ft) has large numbers of burrows and coal fragments, because of which the sandstone has a low permeability and a high clay content (Fig. 8b). Below the burrowed zone, there is a massively bedded zone of Upper Shoreface deposit where the clay content is sharply reduced and grain size and permeability increase up to a depth of 245 ft. This high permeability zone has comparatively fewer burrows. Below the massive bedded zone the quality of the Upper Shoreface deposit deteriorates because of clays associated with burrows and laminations, possibly due to alternating depositional energy cycles. Because of the sedimentological variations there are large swings in permeability values throughout the sandstone (from 245 to 265 ft).

In contrast to sand no. 1, this sandstone (no. 2) has a much higher degree of variation in petrophysical properties resulting from sedimentary and diagenetic features and depositional cycles which create laminations of high and low permeability layers. The higher degree of burrowing in sandstone no. 2 compared to sandstone no. 1 has raised the clay content which has reduced permeability and porosity.

The fluid flow profile in such a reservoir with large-scale permeability stratification is expected to exhibit a significant amount of fingering.

Sand No. 3 (from 281 to 295.5 ft)

The topmost 1 ft of this tidal channel deposit (Fig. 8c) from 280.5 to 291 ft is clayey, has small grain sizes (50 microns) and low permeability (50 mD). Below this zone there is a very clean, high permeability streak where

permeability increases to 250 mD and grain sizes to 300 microns. Further down, the permeability reduces sharply because of carbonate rocks in the shell beds, although the grain sizes in the sandstone are fairly large (around 175-250 microns). These beds are easily identifiable on density logs by their high density readings. The clay content throughout the tidal channel deposit from 281 to 291 ft is moderately high due to mud clasts. The flood tidal delta deposit (below 291ft) is characterized by increasing clay content and decreasing permeability downwards.

Except for the high permeability streak at the top, the remaining parts of sandstone no. 3 appear to be very tight because of carbonate rocks from shell beds, which have reduced effective permeability to very low values. Only the top portion of the reservoir has good permeability for sustained production.

Determination Of Porosity From CT Densities

The estimations of porosity and the clay volumes from the wireline log data provide average values within a certain rock volume and may not have the desired resolution to study the effect of small depositional and diagenetic features. Some of these features may have a profound effect on fluid production in the reservoirs. Therefore, the porosity variations at vertical depth intervals were measured at each quarter of a foot from CT density data. As explained earlier, CT densities provide measurements within a relatively small rock volume (of the order of 50 cm^3) and therefore, should be ideal to study porosity variations associated with geological features of interest.

Comparison of Wireline Log and CT Data

To develop a technique for estimating porosity from the CT data, a comparison between the wireline and the CT density data is required to derive values of certain constants in CT units, such as the matrix density or the shale density, values of which are known only in wireline log units, i.e., in gms/cm^3. Two important differences between the wireline and the CT densities must be emphasized before a comparison between the two sets of data can be made. First, there is a significant difference in the volume of investigation by the two tools, which means that unless the rock is of uniform density some amount of scatter in the crossplot of the two sets of data is expected. This scatter will increase as the spatial heterogeneity of the rock increases. The second difference relates to the environment of measurement. While the pore spaces of the CT-measured cores are air filled, the wireline log measurements were made in rocks whose pore spaces were filled with either formation fluid or drilling mud or a combination of both. The fluid in the pores of permeable formations within the relatively shallow zones in Corehole no. 2 (above the water table) investigated by the tool (less than 1 ft) is mostly mud filtrate (Schlumberger, 1987). This mud filtrate may have a density slightly less than 1 to more than 1.1 gm/cm^3 depending upon salinity, temperature and pressure. For a more accurate correlation of the CT and wireline density, the mud density in the pore spaces in wireline measurements should be replaced by the density of air. A computer program was developed for calculating the density differential required for correcting the density values from the estimated porosities from the density and the gamma ray logs. Figure 9 shows the crossplot of CT and pore fluid corrected wireline densities in Corehole no. 2. The corelation coefficient between the two sets of density values is r = 0.88, which is an improvement over the original correlation obtained without the density correction. A higher degree of correlation was not obtained presumably because of the spatial heterogeneity of rocks in Corehole no. 2.

Porosity Estimation from CT Densities

The porosity of a rock ø, may be estimated from bulk density ρ_b using the following formula (Dewan, 1983; Asquith, 1989).

$$\phi = (\rho_{ma} - \rho_b)/(\rho_{ma} - \rho_f) - V_{sh}\,(\rho_{ma} - \rho_{sh})/(\rho_{ma} - \rho_f) \qquad (1)$$

where ρ_{ma} = matrix density of rocks
ρ_f = fluid density in the pore spaces
ρ_{sh} = density of shale
V_{sh} = volume of shale or clay

Reliable values of all the above densities are known in the Almond Formation (NIPER-529) in gms/cm^3. The straight line relationship shown in Figure 10 was used to obtain the equivalent values of these constants in the CT density (Houndsfields) unit.

Once the values of these constants are known in CT units, porosity may be calculated from the CT densities (which provide the bulk densities) from equation (1) above, provided reliable values of shale volumes can be estimated. The shale or clay volumes may be estimated from the gamma ray logs digitized at 0.5 ft intervals.

Although V_{cl} values are ideally needed at 0.25 ft intervals for calculations with the CT data, it has been observed that careful interpolation will provide acceptable V_{cl} values at 0.25 ft intervals for reliable estimation of porosity. As an example, for a hypothetical case of a sandstone, we assume the following constants:

ρ_{ma} = 2.65 gm/cm^3
V_{sh} = 4%
ρ_b = 2.3 gm/cm^3
ρ_f = 1.00 gm/cm^3
ρ_{sh} = 2.50 gm/cm^3

The calculated porosity for the above rock parameters is 20.84%. If we assume that the actual V_{cl} is 5% instead of 4% the resulting porosity would be 20.75, a very small difference from the earlier value. Therefore, while the clay correction is essential for accurate porosity estimation, small variations of the clay values will cause only very small errors in porosity estimates.

Porosity and Permeability Variations in Sand No. 2

The CT densities in sand no. 2 were used to calculate porosities at 0.25 ft depth intervals from equation (1). The computer program CTPHI calculates clay volumes and porosity from the gamma ray and the density logs and then estimates the porosities from the CT densities and the constants. Figure 10 shows the plot of CT density derived porosities and the minipermeameter measured permeabilities in sand no. 2.

There is generally a good correlation between the porosities and the permeabilities (Figure 10) but some subtle differences in the petrophysical properties of the different sandbodies in sand unit no. 2 may be noted. Although the entire unit has been interpreted as Upper shoreface deposit, the topmost part, from 241 to 245 ft has larger grain sizes, is more massive in character, and has better porosities and permeabilities compared to the lower sandbody, where a larger amount of burrowing with associated clays has been encountered. There is a sharp reduction in permeability in the lower sandstone, although the porosity remains fairly high. This could be because of disconnected pores in the sandbody, such as in rocks with numerous micropores. Compared to the upper zone, the flow characteristics of the lower zone will be much poorer and effective drainage of the reservoir may require appropriate EOR technology based on permeability profile modification.

Discussion

From the analysis of petrophysical property distributions in bar 'F' encountered in Corehole no. 2, the following conclusions may be drawn:

1. The permeability and porosity distributions in the different facies of the nearshore sandstone deposit are highly variable and are strongly controlled by the depositional and diagenetic clays and moderately by grain size. The best permeabilities are always encountered in massive, clean sandstones with low clay content and medium to large grain size.

2. Heterogeneities introduced into the sandstones by the presence of burrows, clay clasts, rooted structures, etc. have the effect of increasing the clay content, and decreasing the permeability. The presence of these sedimentary features results in the development of a high degree of permeability stratification. Enhanced recovery of such a reservoir involving injection of fluid, such as in waterflooding will result in poor fluid recovery.

3. The bounding surfaces of potential reservoirs in this sandstone deposit are usually coal, clay, and carbonate cemented beds which have practically zero permeabilities except when these beds are fractured. These low permeability beds form flow unit boundaries in a fluid propagation profile of the reservoir.

4. The clay content estimated from the gamma ray logs may be on the high side as compared to that of the sandstones in Patrick Draw field. This could be due to the presence of non-clay radioactive minerals and/or the presence of organic remnants that give rise to high gamma ray readings. The amount of non-clay radioactive minerals may be resolved from XRD analysis or from spectral gamma ray logging which gives a quantitative estimate of the potassium, thorium and uranium content in the rocks.

5. An accurate, new technique proposed for estimation of porosity distributions from analysis of CT density data enables us to study the effect of thin zones such as the microporous beds. The porosity estimated from CT data can be integrated with minipermeameter data to study porosity and permeability variations in thin zones, which is not possible from wireline log data because of the averaging effect of the log data.

RECENT GEOCHEMICAL REGIMES IN THE AREA OF COREHOLE NO. 2; THEIR POTENTIAL IMPACT ON MINERALOGY AND PETROPHYSICS OF EXPOSED SHORELINE BARRIER SEDIMENTS.

Introduction

Trends of geochemical mass transport which affect petrophysical properties of ancient shoreline barrier deposits under different geochemical regimes are being sought. Characteristic geochemical processes acting within the deposits exposed to the surface chemical weathering in the unsaturated zone and those in shallow subsurface (under permanent ground water table) are emphasized.

The initial stage of this study on the geochemical processes in the vadose and phreatic zones provides preliminary information leading to more knowledgeable application of petrophysical data collected from outcrops and from shallow drillholes, quarries, aquifers, or mines to improve the characterization of fluid flow units in their oil-bearing analogs.

The potential for recent geochemical modification of petrophysical properties in the upper Almond rock suites exposed on the eastern flank of the Rock Springs Uplift is inferred based on the interpreted geological, geochemical, hydrogeological, and some hydrogeochemical data. The data were collected from investigation of the Corehole no. 2, direct field observations of outcrops, and from other sources such as the U.S.G.S., Wyoming Geological Survey, and Petroleum Data System (PDS BRIN) data file.

An attempt is undertaken to reconstruct the processes acting on the rocks during a period of time preceding measurement of petrophysical properties in the outcrops and the downdip located Corehole no. 2. The investigated outcrops of the upper Almond Formation are internationally recognized by oil companies as representing typical mesotidal shoreline barrier deposits, similar to those producing oil and gas in a number of economic fields in the United States and abroad.

Hydrolysis and oxidation are the primary processes of chemical weathering at and near the land surface. Carbonic acid is one of the primary weathering agents in both unsaturated and saturated zones. The processes cause an efficient dissolution of sulfides, carbonates, silicates and oxides (listed in the order of increasing resistance to chemical weathering). The soluble products migrate with ground water along pathways of ground water movement. Therefore, local hydrogeological conditions play a decisive role in the process of recent geochemical mass transportation and need to be recognized. The recent near-surface processes of dissolution and subsequent precipitation of insoluble products provide a final touch on the mineralogic composition and petrophysical properties of the host rocks after a long sequence of diagenetic alterations starting during their deposition and acting through out burial and uplift stages.

The magnitude of the mineral mass export from the land surface can be roughly estimated by an approximate ratio of the dissolved solids between the average rainfall and the average ground water which is at least 1 to 10. The process of mass transport acting through geologic time removes from one area and re-precipitates in another an appreciable amount of mineral substances. In the conditions of the water table the ground water transports the dissolved solutes from the land surface through the unsaturated zone to the ground water table (vertical transport) and from the recharge to the discharge area (dominantly horizontal transport).

In general, the relatively minor minerals forming clastic rocks such as plagioclase, amphibole, pyroxene, and biotite are easily weathered; and their leaching may increase the porosity and permeability in proportion to their original content. Potassium-feldspar and muscovite are moderately stable, and quartz is very stable (Levinson, 1974). During chemical weathering, the major mineral-forming elements such as Na, Ca, K, Fe, Mg Mn, Si, Al, S, and C a number of minor and trace elements (e.g., Sr, Ba, F, Cl, Li, Rb) are set free and transported with water molecules mostly in ionic form.

Iron and manganese oxides and sulfides, sulfates, carbonates, and clay minerals are volumetrically the most important precipitates along the pathway of ground water and within the fluctuation zone of the ground water table. Some of those precipitates which are observed macro- and microscopically in different sections of the core from Corehole no. 2, can be of the recent origin related to weathering of rocks exposed to the atmosphere and to shallow ground waters. The trend and magnitude of recent geochemical alterations of the ancient reservoir analogues in outcrops or shallow subsurface (like the outcrop G and the Corehole no. 2, respectively) depend on the length of exposure time, position within local and regional hydrologic cycle, and local climatic conditions.

The magnitude of the mineral mass transport due to specific geochemical reactions, which are responsible for alterations of the petrophysical properties of rocks, cannot be quantified at this stage of the project. Geochemical simulation of water evolution along the ground water flowpath would be needed to quantify products of the water-rock interaction. The simulation would have to be based on quantified hydrogeochemical data collected upstream and downstream of the ground water flow in the area of interest.

Regional Hydrogeochemistry

The following discussion of the regional hydrogeochemical conditions in the Rock Springs Uplift provides a link between the investigated shallow zone of geochemical processes (this project) and those prevailing in Patrick Draw reservoir at depth of about 4,600 ft and described by Szpakiewicz (1993). Szpakiewicz and Collins (1985) demonstrated on hydrogeochemical cross-sections through the Greater Green River Basin that the descending meteoric waters (HCO_3-Na type) gain salinity with depth and change their chemical composition to HCO_3-Cl-Na, and Cl-HCO_3-Na type (sometimes including sulfates in excess of 20% miliequivalents) in the mixing zone (usually not exceeding 3,000 ft). Similar distributions of hydrochemical facies has been shown on the cross-section from the Almond Formation outcrops down to about 2,500 ft in the Washakie Basin updip of Patrick Draw field.

The distribution of chloride concentrations versus total dissolved solids (TDS) in the general area east of the Rock Springs Uplift follow the ocean water dilution-concentration line defined by the equation: TDS = 1.805 Cl-. This suggests an ascension of relict, connate waters from deep-seated marine formations into the shallower non-marine sections of the basin, followed by dilution with fresh meteoric waters, and an alteration caused by interaction with the surrounding rocks and hydrocarbons (Szpakiewicz and Collins, 1985). A slight parallel departure from the sea water dilution line is caused by a gain of the anions HCO_3^- or SO_4^{2-} (points below the line), or cations, mostly Ca^{2+} (points above the line). Some points depart significantly from the line indicating advanced rock-water interaction (Szpakiewicz and Collins, 1985).

Ground waters which are dominantly of meteoric origin, are located within the uppermost portions of the basins, and have low salinity (below 5 g/l TDS). The waters, typically are: (1) deficient in chloride (of HCO_3-Cl-Na, HCO_3-Na, SO_4-Cl-Na chemical types), (2) have a geochemical alteration index (rNa/rCl) higher than 1.6, indicating unfavorable conditions for oil survival, and (3) have a reductivity index ($rSO_4 \times 10^3/rCl$) much higher than 200 indicating the oxidizing environment which confirm the unfavorable conditions for economic accumulations of oil (Szpakiewicz and Collins, 1985).

Similar relationships were observed when the log Na^+ concentrations versus log Cl^-, concentrations were plotted. The formation water data again closely follows the sea water dilution/concentration line, expressed by the equation: log Cl^- = 1.064 log Na^+. Points located far off this line on the right, represent marine waters from relatively isolated environments, where Na^+ from solution was exchanged with Ca^{2+} in the surrounding clay rocks (mostly shales), mudstones or carbonaceous sandstones. The points located left of the line represent waters which gained mostly bicarbonates and sometimes sulfates while chloride was depleted. This can be attributed to the leaching processes and/or the interaction with organic matter. The lower concentrations of TDS, and the divergence from the ocean water line is interpreted as an increased contribution of meteoric waters to the formation fluids (Szpakiewicz and Collins, 1985).

In the shallow geochemical zone where meteoric ground waters descend, the dominantly oxidizing conditions destroy most hydrocarbon accumulations. East of the Rock Springs Uplift at depths of 2,500-3,000 ft, however, the geochemical conditions gradually become favorable for generation of biogenic methane and for oil survival (Szpakiewicz and Collins, 1985). At depths greater than 3,300 ft in the Almond Formation of Patrick Draw oil and gas field a documented strong hydrogeochemical anomaly indicates compartmentalization of reservoir fluids. High salinity formation waters (up to 72,000 mg/l TDS) of different chemical composition were documented on top of much less saline waters in the oil producing sandstones (Szpakiewicz, 1993).

Characteristics of Hydrogeologic Conditions in Shallow Zones

The purpose of reconstructing the hydrogeologic conditions in the general area of Corehole no. 2 has been to improve the understanding of flow characteristics in the examined core with emphasis on the role of the geochemical alterations of sediments. These sediments near the bounding surfaces indicate major changes in the environment of deposition and possible periods of erosion. Our objective is to indicate trends in recent geochemical alterations of the Upper Almond Formation outcrops on the southeast flank of the Rock Spring Uplift caused by the rock-water interaction processes acting within the unsaturated zone, in the transition zone, and downdip below the ground water table in the permanently saturated zone.

In the unsaturated zone, the climate-specific physical and chemical weathering processes and products affect the petrophysical properties of the Almond Formation rocks exposed in outcrop. Different geochemical conditions and the resulting alteration products can be expected in the saturated zone, i.e., under the ground water table level in Corehole no. 2. Corehole no. 2 was drilled about 0.5 mile downdip from the outcrops compared.

Hydrogeologic data and signatures of resistivity logs from 41 boreholes drilled on the southeastern flank of the Rock Springs Uplift have been examined for determination of unsaturated and saturated zones (depths to ground water table) and for characteristics of ground water flow in the Almond Formation sediments. A ground water pressure head map has been constructed showing equipotential lines along which the pressure head is the same (figure 4.1). The map allows determination of directions of ground water flow and the definition of hydraulic gradients in the area.

Infiltration of fresh meteoric waters through the unsaturated zone, locally thicker than 500 ft and occasionally up to 900 ft, has been documented based on the resistivity and conductivity logs in a number of drillholes along the belt of the Almond Formation outcrops near Corehole no. 2. The deep descent of meteoric waters, particularly at the edges of sedimentary basins, is not uncommon in the Rocky Mountain region (Szpakiewicz and Collins, 1985). For example, fresh waters from recent infiltration were encountered in the Lower Tertiary Wasatch Formation of the Pinedale Unit, Green River Basin at 2,300 ft. The carbon-14 age was estimated at 20,800 years B.P. (Dinwiddie, 1973). In the Parriette Bench field (Green River Formation in the Uinta Basin) the authigenic carbonate cement was formed at low temperatures in the presence of recent or paleoinfiltrated meteoric waters at a depth of about 6,000 ft, as indicated by stable isotope data (Pitman, et al. 1982).

The near surface exposure of the Almond Formation, in Corehole no. 2 on the southeastern flank of the Rock Springs Uplift, shows the ground waters are generally flowing toward southeast with local divergence of flow direction to the east (Fig 11). The upper Almond Formation exposures strike NE-SW in the area. The ground water flows generally downdip of the local geological formations. Depth to ground water table varies from less than 25 ft in low areas (valleys, gulches, and draws) to more than 500 ft in morphological highs. Differences in terrain elevations exceed 1,000 ft in the mapped area. There is no indication of obvious natural surface discharge zones of ground waters such as perennial streams, permanent springs, or ground water seeps. Most streams temporarily gather the local surface runoff water before it evaporates and partially infiltrates to the subsurface. A possible water recharge area for the regional aquifer must be located somewhere on the Rock Springs Uplift within the most elevated zones of the exposed Rock Springs and Erickson sandstones. Therefore, most of the ground water entering the upper Almond shoreline barrier deposits below the ground water table flows on its way down the hydraulic gradient (southeastward and/or eastward) through rocks of different lithologies and origins including the mostly continental lower Almond Formation with the abundant coal seams and the gypsiferous lagoonal and bay layers. The approximate hydraulic gradient in the area has been calculated from the piezometric contour map (Fig 11) and varies between 133 and 166 ft/mi in the general area. Based on these data and on the assumed hydraulic conductivities (for the upper Almond the K value of 4×10^{-5} cm/sec is probably a reasonable approximation) the velocity of ground water flow, water migration paths, and the approximate time of water residence in subsurface can be determined. The data indicate that the ground waters encountered in the upper Almond deposits gain their chemical composition flowing downgradient through the Rock Springs, Erickson, and the lower Almond sediments to the upper Almond Formation. The computed approximate residence time of water molecules in the subsurface before reaching the Corehole no. 2 may be close to 1.5 and 2.0 million years.

Direction of Geochemical Alterations in Shallow Zones

In the shallow geochemical zone where Corehole no. 2 is located, the exporting mineral mass transport resulting from breakdown of carbonates, silicates, and sulfides should take place along the ground water flow paths. Different types of abundant iron-containing minerals such as sulfides (pyrite, marcasite, chalcopyrite, etc.) and carbonates (siderite and ankerite) are expected to be transformed in insoluble form such as iron and manganese oxides, clay minerals, sulfates, carbonates, and silicates which usually precipitate as cements, coatings on mineral grains, or residual limonitic material (Levinson, 1974).

Significant change of geochemical conditions from the unsaturated zone (in outcrops) through the transition zone of fluctuating ground water table and capillary fringe zone down to the permanently and continuously saturated zone leaves an imprint on petrophysical properties of rocks and their ability to conduct fluids. However, at this stage of the project a quantification of the processes by geochemical mass balance in the three geochemically different environments is difficult because detailed ground water analyses and equivalent rock mineralogic analyses are not available. Products of the geochemical reactions described below should be confirmed by XRD analyses and petrographic analyses of thin sections taken from selected intervals of Corehole no. 2 near bounding surfaces. The preliminary geochemical and petrographic results will hopefully indicate the most promising directions for deeper investigation of that intriguing and practically important problem which may affect many other petroleum related investigations involving outcrops. For example, upto 34% carbonate (mostly non-calcite) cement were found in some samples from the saturated zone of Corehole no. 2 (Table 3). It would be useful to compare the amount of carbonate and other authigenic cements found in the saturated zone with those in the stratigraphic equivalent within

the unsaturated zone of outcrop G. This problem is one of the candidates suggested for further investigation during the extention of this project beyond the preliminary stage.

Hydrolysis of carbonates mobilizes metals and increases alkalinity and the amount of bicarbonates in solution. Silicates (such as orthoclase) are also mobilized by hydrolysis and can be transformed to kaolinite. In many cases (when water is abundant) common processes are of primary importance for the alteration of mineralogic and petrophysical properties.

Two other important mineral transformations deserve to be singled out for the purpose of this study, namely, oxidation of sulfides producing goethite and lepidocrocite (both become the main constituents of limonite cement) and sulfuric acid, according to the following combined (net) reaction:

$$4FeS_2 + 15O_2 + 10H_2O = 4FeO(OH) + 8H_2SO_4 \quad (2)$$

The generated sulfuric acid will further react with the rock-forming carbonates (oyster shells, calcite cement, etc.) producing gypsum and carbonic acid

$$CaCO_3 + H_2SO_4 + 2H_2O = CaSO_4 2H_2O + H_2CO_3 \quad (3)$$

The resulting carbonic acid contributes to further dissolution of carbonates which can freely migrate out of the shallow system in the form of dissolved bicarbonates $Ca(HCO_3)_2$.

Biological weathering, such as the bacterial oxidation of pyrite in the shallow zone by aerobic microorganisms as well as reduction of sulfates to hydrogen sulfite by anaerobic bacteria in deeper zone, may also contribute to mineralogical and petrophysical changes. The latter process causes metals to re-precipitate from the water solution along the migration path of ground water.

Many of the near-surface weathering alterations in the unsaturated zone require an abundance of water as a dissolution agent and a carrier of the dissolved mineral substance to the ground water table. Therefore, they may be less advanced in Wyoming's semi-arid climate with its low annual precipitation. For example, feldspars are typically unstable under weathering conditions. However, little hydrolysis of feldspar grains is expected in the Wyoming's high topography and dry climate in comparison with low topography and humid climate where nearly all the feldspar would be weathered away.

Recent Hydrogeological and Geochemical Conditions in Corehole No. 2

Corehole no. 2 is located at the bottom of Big Flat Draw near its outlet to the Salt Wells Creek valley at a ground elevation of 6,790 ft on the downdip side of Roehler's "bar G" and "bar F" of the upper Almond shoreline barrier rock suites (Roehler, 1988). The deposits crop out at a distance of less than half a mile NW of Roehler's outcrop G (Roehler, 1988). The detailed geologic profile of outcrop G and the correlation of the shoreline barrier facies interpreted in outcrop G with those in the Corehole no. 2 has been shown elsewhere in this report.

The largest potential for differences in the petrophysical properties of the genetically equivalent rocks (facies) in outcrop and in Corehole no. 2 lie in the different geochemical environments that the two rock suites were subjected to for millennia. The outcrop is a morphologically elevated feature located entirely within the unsaturated zone where the meteoric waters infiltrate, dissolve, evaporate, precipitate, freeze, and mechanically disintegrate rocks. Most of the core recovered from Corehole no. 2, however, was located below the ground water table, i.e., within zone of flowing water down dip of the hydraulic gradient of the regional aquifer.

The following vertical water saturation zones have been identified in Corehole no. 2 based on core observation and resistivity log readings: 1) the vadose zone (unsaturated zone above the capillary fringe and seasonal fluctuation zone), 2) the transition zone (where ground water table fluctuates seasonally), and 3) the phreatic zone (permanently saturated zone below the lowest level of the ground water table). The first two zones are highly oxygenated, within the aquifer the oxygen becomes gradually exhausted down the flow path. That is why most of the dissolved mineral substances can be transported in solution downstream to a drainage area. Some solutes may easily precipitate, within the capillary fringe zone and the seasonal fluctuation zone of the ground water table. Examination of the core clearly indicates a strong staining by a spectrum of oxides within the tidal channel sandstone sequence which extends from the top of the recovered core at 25 ft down to about 44 ft. Typically, such an oxygenation takes place within a zone of seasonal fluctuations of ground water table.

The resistivity and conductivity logs from Corehole no. 2 strongly indicate the position of the ground water table at a depth not greater than 25 ft at the time of drilling and logging the hole. Below this depth the resistivities are lower than 100 ohm-m, the values characteristic for the saturation with fresh water in other holes logged in the general area and reported by McClung, et al., 1983 (Table 5). This interpretation is also consistent with the position of the regional ground water table interpreted in the area of Corehole no. 2 from the ground water pressure head map

covering the larger area of the Almond Formation outcrops on the southeastern flank of the Rock Springs Uplift (Fig 11).

An interval of fluctuating ground water table cannot be defined from the existing description of hydrologic conditions in Corehole no. 2 and from the available geophysical logs. However, visual examination of the core clearly indicates a strong staining by a spectrum of oxides in the tidal delta ramp sandstone sequence which extends from the top of the recovered core at 25 ft down to 44 ft in Corehole no. 2. Typically the oxygenation takes place within a zone of seasonal fluctuation of the ground water table. Siderite, for example, which may be a quite common carbonate cement precipitating at the initial stage of diagenesis in barrier island sediments has not a chance to survive in the highly oxidizing environment of the fluctuating ground water table, and most probably would be converted to ferric oxide. Many of the iron-stained and iron-cemented sandstones result from the alteration of siderite. MnO_2 is another example of the same process. Pyrite and marcasite (otherwise quite common in the Almond Formation) are very easily weathered and would not be expected either in the unsaturated zone or in the immediate area of the ground water table. Instead, thin coatings of native sulfur are commonly observed in the Almond outcrops in coal cleats and small cracks in mudstones. Common local enrichment of ground waters in sulfates (SO_4^{2-}) in the general area may account for the oxidation of iron and manganese sulfides. The drastic drop of pH due to produced sulfuric acid in reaction would trigger decomposition of more sulfides in the system. Hydrolysis of carbonates and silicates, which releases KOH (increasing alkalinity) provides necessary pH balance to the environment.

Based on visual examination of core, log signatures, and interpretation of the piezometric map constructed for the purpose of this project the ground water table fluctuated for millennia in the area of Corehole no. 2 at a depth range between at least 25 ft and 44 ft below land surface. The 20 ft thick interval of the shoreline barrier sandstones was affected mostly by oxygenation of iron and manganese minerals and other cyclic precipitation/dissolution processes.

The core interval adjacent to the examined bounding surface at a depth of 282 ft is located well below the zone of possible fluctuation of the ground water table, i.e., it was influenced only by the processes acting in a permanently and fully saturated (aquifer) zone under predominantly reducing conditions; because most of the oxygen would have been depleted along the migration path from the recharge area. The effects of geochemical processes in Corehole no. 2 should be different from those in the unsaturated zone near the equivalent bounding surface at the outcrop G. Thus, we expect that the detailed mineralogy and the measured petrophysical properties such as porosities, permeabilities, and capillary pressures should also be different in the two environments.

This stage of study provides necessary background for attempted determination of a potential influence of the present day composition of ground waters on the modification of petrophysical properties of the upper Almond facies and bounding surfaces in Corehole no. 2. In most cases the upper Almond sequence is being flushed with waters of low mineralization, rarely exceeding 1,000 mg/l of NaCl equivalent. The resistivity logs in the area rarely indicate R_W values as low as 8 to 10 ohm-m. Usually, R_W's at 200 ft and 300 ft (in the saturated zone) is between 23 ohm-m to 60 ohm-m (Table 5). In some drillholes fresh water was indicated by resistivity log at depths of 700 to more than 800 ft, and even 930 ft in the drillhole CNRE-8 (McClung, et al. 1983). In Corehole no. 2 the R_W at a depth of 100 ft is 28 ohm-m, at 200 ft R_W is 60 ohm-m, and starts oscillating between 30 and 90 ohm-m from 280 ft downward to the TD (529 ft). The variation of resistivity values, particularly below 280 ft, indicates a higher heterogeneity of rocks and probably more differentiation of interstitial electrolytes.

In the Corehole no. 2 at depth of about 280 ft, where the possible marine flood surface marks the transition from the backbarrier tidal channel-related coquina beds to the overlying marine shoreface faces, the resistivity log reads 45 ohm-m. Lower than that resistivity values of 10, 20, and 30 ohm-m were monitored at depths 62 to 90 ft, 180 ft, and 300 ft, respectively. There are higher resistivities (80 to 100 ohm-m) monitored in the highly calcite cemented layers which immediately underlie the flooding zone at 280 ft. The resistivity of the section overlying the flooding zone varies between 60 and 70 ohm-m. The zone represents marine shoreface facies. Petrographic and XRD results indicate a mineralogic reason for the lower resistivities near the flooding surface at 280 ft and at 62-90 ft, 180 ft, and 300 ft. However, if lower resistivity mineralogy is not obvious there, than we should assume presence of lower resistivity (higher TDS) fluids flowing through those intervals. If this is the case, all four intervals should be considered as preferential flow units in the vertical system.

Low resistivity values in the interval from about 30 ft to 50 ft may generally correspond with the fluctuating ground water table interval (transition zone). Because the well was drilled in July there is a good chance that the ground water level was still at the annual highest level, it is quite reasonable to assume that the whole transition interval was fully saturated with water at that time. Considering the strong possibility of dissolution of the local evaporites which precipitated in the transition zone at the lowest water table level, the resistivity measured in July should be low.

The specific composition of interstitial waters at different depth intervals in Corehole no. 2 is not known. There is an indication, however, that the waters may contain enhanced amounts of bicarbonates and local sulfates.

Certain easily soluble minerals which are in solution below the ground water table, such as nahcolite ($NaHCO_3$), dawsonite ($NaAl(CO_3)(OH)_2$), and trona ($Na_3(CO_3)(HCO_3)2H_2O$), may equally easily re-precipitate in dry climates when the solution would intersect the land surface or contact the transition zone of fluctuating the ground water table. Otherwise, there is a chance that they migrate in solution increasing its electrolytic properties. It should be kept in mind that specific conductance of sodium or calcium bicarbonate solutions (which most probably dominate) is much lower (resistivity higher) than sodium-chloride solutions (Driscoll, 1986). Therefore, the resistivity measured in Corehole no. 2 may not reflect fresh (potable) waters but actually the ground waters of slightly enhanced salinities.

Discussion

The study of geochemical alterations leading to the mineralogic and petrophysical changes within the vadose and phreatic zones in the area of the Almond Formation outcrops and the Corehole no. 2 (drilled downdip about half a mile from surface exposures) provides a chance for more reliable application of petrophysical data collected from outcrops, quarries, and shallow drillholes to improve characterization of fluid flow units in oil-bearing analogs.

On the east flank of the Rock Springs Uplift, the descending meteoric waters of HCO_3-Na type gain salinity with depth and change their chemical composition to HCO_3-Cl-Na, and Cl-HCO_3-Na type (sometimes also including sulfates in excess of 20% miliequivalents) in the mixing zone, usually not exceeding depth of 3,000 ft. In the shallow geochemical zone of descending meteoric waters, prevailing oxidizing conditions are highly unfavorable for survival of hydrocarbon accumulations.

In the area of Corehole no. 2, the ground waters flow southeast with local divergence of flow direction to the east, generally downdip of the local geologic strata. Depth to ground water table varies from less than 25 ft in low areas (valleys, gulches, and draws) to more than 500 ft in morphological highs.

The approximate hydraulic gradient of the free ground water table (Fig 11) varies between 133 and 166 ft/mi in the general area of Corehole no. 2.

The hydrogeologic calculations indicate that the ground waters encountered in the upper Almond deposits of Corehole no. 2 infiltrate the Rock Springs Uplift and gain their chemical composition flowing downgradient through the Rock Springs, Erickson, and the lower Almond sediments to the upper Almond Formation. The approximate computed residence time of water molecules in subsurface before reaching Corehole no. 2 is in the range of 1.5 to 2.0 million years.

The resistivity and conductivity logs from Corehole no. 2 strongly indicate the position of the ground water table at a depth not greater than 25 ft at the time of drilling and logging the hole. There is strong indication from core staining with oxides, that the ground water table fluctuated for millennia at depth range between at least 25 ft and 44 ft below land surface. Deeper than that, rocks were always fully saturated with the ground water flowing downgradient toward the center of the Washakie Basin. According to resistivity variations from below 30 ohm-m to more than 90 ohm-m, the ground water in the phreatic zone is fresh or slightly saline of non-chloride-sodium composition. In the shallow geochemical zone where Corehole no. 2 is located, the mineral mass transport results mainly from breakdown of carbonates, silicates, and sulfides along the ground water flow paths.

Hydrolysis of carbonates mobilizes metals and increases alkalinity and the amount of bicarbonates in solution. Silicates (including orthoclase) are also mobilized by hydrolysis and are transformed to kaolinite. The processes are probably of primary importance for mobilization of minerals and petrophysical changes in the vadose and phreatic zones.

Oxidation of sulfides produces limonite cement and sulfuric acid. The generated sulfuric acid reacts with rock-forming carbonates such as oyster shells, calcite cement, etc. producing gypsum and carbonic acid. The carbonic acid contributes to further dissolution of carbonates which can freely migrate out of the shallow system in the form of dissolved bicarbonates $Ca(HCO_3)_2$.

Different types of ubiquitous iron-containing minerals such as sulfides (pyrite, marcasite, chalcopyrite, etc.) and carbonates (siderite and ankerite) are expected to be transformed into insoluble forms such as iron and manganese oxides, clay minerals, sulfates, carbonates, and silicates which usually precipitate as cements, coatings on mineral grains, or residual limonitic material effectively plugging pores and pore throats.

Iron and manganese oxides and sulfides, sulfates, carbonates, and clay minerals are volumetrically the most important potential precipitates along the ground water pathway and within the fluctuation zone of the ground water table.

The geochemical reactions and their products in the vadose and freatic zones deserve attention because of their potential impact on the petrophysical properties of commonly investigated analogs of deep hydrocarbon reservoirs. Although they cannot be quantified at this stage of the project, the high probability of their occurrence helps the petrophysicists and petrographers interpret their results and orient their studies toward directions indicated by geochemistry. Hopefully, the preliminary geochemical investigation indicates some promising directions for

deeper investigation of this intriguing and practically important problem which may affect many other petroleum related investigations involving outcrops.

It should be kept in mind, however, that hydrolysis in the unsaturated zone requires abundance of water as a dissolution agent and carrier of dissolved substance. Therefore, it may be less influential in the Wyoming's semi-arid climate with low annual precipitation than the oxidation processes.

REFERENCES

Allen, J. R. L., 980, Sand Waves: A Model of Origin and Internal Structure: Marine Geology, v. 26, p. 281-328.

Asquith, G. B., 1989, Log Evaluation of Shaley Sandstones: A Practical Guide: AAPG Continuing Educaiton Series no.31, Tulsa, OK, 596 p.

Brookfield, M. E., 1977, The Origin of Bounding Surfaces in Ancient Aeolian Sandstones: Sedimentology, v. 24, p. 303-332.

Crain, E. R., 1986, The Log Analysis Handbook: PennWell Books, Tulsa, OK, p. 115-247.

Dewan, J. T., 1983, Essentials of Modern Open-Hole Log Interpretation: PennWell Books, Tulsa, OK, 265 p.

Dinwiddie, G., 1973, Hydraulic Testing and Sampling of Water Well Number 2. Project Wagon Wheel, Sublette County, Wyoming: U.S.G.S. Denver.

Dott, R. H., Jr., and Bourgeois, J., 1982. Hummocky Stratification: Significance of its Variable Bedding Sequences: Geological Society of America Bulletin, v. 93, p. 663-680.

Driscoll, F.G., 1986, Groundwater and Wells: Johnson Filtration Systems Inc., St. Paul, Minnesota 55112, 1088 p.
Folk, R. L., 1968, Petrology of sedimentary rocks: Hemphill's, Austin Texas, 170 p.

Houseknecht, D. W., 1984, Influence of Grain Size and Temperature on Intergranular Pressure Solution, Quartz Cementation, and Porosity in a Quartzose Sandstone: Jour. Sed. Petrol., v. 54, p. 384-361.

Jackson, S.R. and V. Rawn-Schatzinger, 1993, Data From Selected Almond Formation Outcrops, Sweetwater County, Wyoming. DOE Report NIPER-724, November, 1993.

Kocurek, G., 1988, First-Order and Super Bounding Surfaces in Eolian Sequences - Bounding Surfaces Revisited: Sedimentary Geology, v. 56, p. 193-206.

Levinson, A.A., 1974, Introduction to Exploration Geochemistry: Applied Publishing Ltd. Calgary, 612 pp.

McClung, J.M., J.D. Gardner, A.P.Boresi, and L.E.Borgman, 1983, Geophysical Logs, Lithologic Description, and Coal Analyses from Coal Test Holes Drilled in 1982 in the Salt Wells and Kemmerer Areas, Sweetwater and Uinta Counties, Wyoming: Report of Investigation no. 24, The Geological Survey of Wyoming, Laramie, Wyoming, 124 p.

Miall, A.D., 1988, Reservoir Heterogeneities in Fluvial Sandstones: Lessons from Outcrop Studies, AAPG Bulletin v.72, no. 6, p. 1761.

Miall, A.D., 1991, Hierarchies of Architectural Units in Terrigenous Clastic Rocks, and Their Relationship to Sedimentation Rate, *in* Miall, A.D. and N. Tyler, eds., The Three Dimensional Facies Architecture of Terrigenous Clastic Sediments and Its Implications for Hydrocarbon Discovery and Recovery, SEPM (Society for Sedimentary Geology) Concepts in Sedimentology and Paleontology, v.3, Tulsa, OK.

Miall, Andrew D., 1986, Facies Architecture in Sedimentary Basins: The Decline and Fall of the Vertical Profile Analysis: (abs.) AAPG Bulletin v.70, no. 11.

Mutti, E., and Normark, W. R., 1987, Comparing Examples of Modern and Ancient Turbidite Systems: Problems and Concepts, *in* Leggett, J. K., and Zuffa, G. G., eds., Marine Clastic Sedimentology: Concepts and Case Studies: Graham and Trotman Ltd., London, p. 1-38.

National Instgitute for Petroleum and Energy Research, 1993, Quarterly Technical Report for April-June 1993 . v. II, Energy Production Research, DOE Report, NIPER-700.

National Institute for Petroleum and Energy Research, 1991, Quarterly Technical Report for January 1 - March 31, 1991. v.II, Energy Production Research, DOE Report, NIPER-529, May 1991, p. 1-4.

Pettijohn, F. J., P. E. Potter, and R. Siever, 1972, Sand and Sandstone: N.Y., Springer-Verlag, 618 p.

Pitman, J., T. Fouch, and M. Goldhaber, 1982, Depositional Setting and Diagenetic Evolution of some Tertiary Unconventional Reservoir Rocks, Uinta Basin, Utah: AAPG Bull, v. 66, no. 10, p. 1581-1596.

Roehler H.W., 1988, The Pintail Coal Bed and Barrier Bar G - A Model for Coal of Barrier Bar - Lagoon Origin, Upper Cretaceous Almond Formation, Rock Springs Coal Field, Wyoming: U.S. G. S. Prof. Paper 1398, p.1-60.

Roehler, H. W., 1988, The Pintail Coal Bed and Barrier Bar G - A Model for coal of barrier bar-lagoon origin, Upper Cretaceous Almond Formation, Rock Springs Coal Field, Wyoming: U.S. Geological Survey Professional Paper 1398, 60 p.

Schlumberger Educational Services, 1987, Log Interpretation Principles/Application: Houston, TX.

Sharma, B., 1992, Petrographic Correlations and Mathematical Analysis of Log Signatures for Clay Identification: DOE Report NIPER-589, p. 1-14.

Shurr, G. W., 1984, Geometry of Shelf-Sandstone Bodies in the Shannon Sandstone of Southeastern Montana, *in* Tillman, R. W., and Siemers, C. T., eds., Siliciclastic Shelf Sediments: Society of Economic Paleontologists and Mineralogists Special Publication 34, p. 63-83.

Szpakiewicz, M., 1993, Application of Hydrogeochemical Techniques to Reservoir Characterization : *In* Integration of the Geological/Engineering Model with Production Performance for Patrick Draw Field, Wyoming. Jackson, S. R., et al. DOE Report, NIPER-634, p.13-40.

Szpakiewicz, M., and A. G. Collins, 1985, Hydrochemical study of the Upper Cretaceous and Lower Tertiary Formations in the Uinta, Piceance, and Green River Basins: Implications for oil-and gas-related problems: DOE Report, NIPER-95, 70 p.

Wilson, J. C., and E. F. McBride, 1988, Compaction and porosity evolution of Pliocene sandstones, Ventura Basin, California. AAPG Bull., v. 72, p. 664-681.

TABLE 1
Hierarchies of architectural units in clastic deposits. After Miall (1991)

Group	Time scale of proc. (yrs)	Examples of processes	Instan-taneous sed. rate (m/ka)[1]	FLUVIAL, DELTAIC Miall	EOLIAN Brookfield, Kocurek	COASTAL, ESTUARINE Allen	SHELF Dott and Bourgeois, Shurr	SUBMARINE FAN Mutti and Normark
1	10^{-6}	burst-sweep cycle		lamina	grainflow grainfall	lamina	lamina	
2	10^{-5} -10^{-4}	bedform migration	10^{5}	ripple (microform) [1st-order surface]	ripple	ripple [E3 surface]	[3-surf in HCS]	
3	10^{-3}	diurnal tidal cycle	10^{5}	diurnal dune incr., react. surf. [1st-order surface]	daily cycle [3rd-order surface]	tidal bundle [E2 surface]	[2-surf in HCS]	
4	10^{-2} -10^{-1}	neap-spring tidal cycle	10^{4}	dune (mesoform) [2nd-order surface]	dune [3rd-order surface]	neap-spring bundle / storm	HCS sequence [1-surf]	
5	10^{0} -10^{1}	seasonal to 10 yr flood	10^{2-3}	macroform growth increment [3rd-order surface]	reactivation [2nd, 3rd-ord surfaces, annual cycle	yer	HCS sequence [1-surface]	
6	10^{2} -10^{3}	100 year flood	10^{2-3}	macroform, e.g. point bar levee, splay [4th-orde surface	er	sand wave field, washover fan	[facies pack-age (V)]	macroform [5]
7	10^{3} -10^{4}	long term geomorphic processes	10^{0}-10^{1}	ch [surfa	aa, erg [1st-order, super surface]	sand-ridge, barrier island, tidal channel	[elongate lens (IV)]	minor lobe, channel-levee [4]
8	10^{4} -10^{5}	5th-order (Milankovitch) cycles	10^{-1}	channel belt [6th-order surface]	erg [super surface]	sand-ridge field c-u cycle	[regional lentil (III)]	major lobe [turb. stage: 3]
9	10^{5} -10^{6}	4th-order (Milankovitch) cycles	10^{-1}-10^{-2}	depo. system, alluvial fan, major delta	erg [super surface]	c-u cycle	[ss sheet (II)]	depo. system [2]
10	10^{6} -10^{7}	3rd-order cycles	10^{-1}-10^{-2}	basin-fill complex	basin-fill complex	coastal-plain complex	[lithosome (I)]	fan complex [1]

Hierarchical subdivisions of other authors are given in square brackets.
Names of authors are at head of each column.
[1]Meters per 1,000 years.

TABLE 2

Sample depth, lithology and tentative depositional facies for petrographically analyzed samples from Almond Corehole no. 2

Depth, ft	Lithology	Depositional Facies
274.7	Feldspathic Litharenite	Abandoned Channel Fill
282.2	Feldspathic Litharenite	Transition at top of Tidal Channel
282.3	Feldspathic Litharenite	Transition at top of Tidal Channel
282.4	Feldspathic Litharenite	Transition at top of Tidal Channel
290.5	Feldspathic Litharenite	Tidal Channel
291.1	Litharenite	Flood Tidal Delta
291.2	Litharenite	Flood Tidal Delta
291.6	Feldspathic Litharenite	Flood Tidal Delta

TABLE 3

Composition and packing data for samples from Almond Corehole No. 2. Q bulk %, F bulk %, RF bulk = quartz, feldspar, and rock fragment content of bulk rock; Q + F + R = 100%; Tot = total; dol = dolomite; fn - fine grained; CI = contact index; TPI = tight packing index; PCØ = porosity from thin section point counts; R_{50} median throat radius from mercury porosimetry.

Depth, ft	274.7	282.2	282.3	282.4	290.5	291.1	291.2	291.6
Grain size, μ	65	170	220	240	230	200	165	155.00
Sorting	well	mod+	mod	mod+	well	well	well	well
Roundness	A-Sa	Sr-Sa	Sa-Sr	Sa-Sr	A-Sr	Sr	Sr	Sr
Q bulk, %	40.0	32.7	28.8	34.2	30.9	34.0	43.6	42.8
F bulk, %	12.1	11.2	10.8	13.1	4.5	8.8	6.8	11.6
RF bulk, %	18.1	19.2	14.0	21.9	9.4	24.4	20.8	16.4
Q, %	57.0	51.8	53.7	49.4	68.9	50.6	61.2	60.5
F, %	17.2	17.7	20.1	18.9	10.1	13.1	9.6	16.4
R, %	25.8	30.5	26.1	31.7	21.0	36.3	29.2	23.2
Matrix, %	0.0	0.4	0.4	0.8	0.0	0.2	1.6	0.0
Tot cement, %	16.3	28.5	34.5	20.9	40.0	14.1	22.6	16.4
Carbonate cement, %	14.7	23.8	32.4	11.6	33.6	6.0	16.4	12.8
Calcite cement, %	0.0	0.00	0.00	0.00	29.10	0.01	0.00	0.00
Coarse dol cement, %	0.0	6.9	2.0	3.5	0.0	0.0	0.0	2.8
Fn dol cement, %	14.7	16.9	30.4	8.1	4.5	6.0	16.0	10.0
Tot dol, %	14.7	23.8	32.4	11.6	4.5	6.0	16.0	12.8
Clay cement, %	0.4	3.8	0.8	8.8	0.0	5.6	6.4	0.0
Tot clay, %	15.9	8.4	5.7	15.6	0.8	10.6	14.6	14.6
CI					1.49	3.40	3.12	2.86
TPI					0.39	2.44	2.32	3.96
PCØ, %	15.1	5.0	7.2	8.8	3.0	11.2	4.4	8.0
R_{50} throat, μ	2.2	1.7	3.5	2.4	8.0	1.8	1.7	1.7

TABLE 4

X-ray diffraction mineral abundances of samples from Almond Corehole no.2.

	Sample Depth (ft)			
Mineral Constituents	**274.7**	**282.4**	**291.1**	**291.2**
Quartz	89	85	83	80
Plagioclase	1	1	1	1
K-Feldspar	2	5	3	3
Calcite	0	Tr	6	8
Dolomite	4	4	3	4
Siderite	Tr	Tr	Tr	Tr
Anhydrite	Tr	Tr	Tr	Tr
Pyrite	Tr	Tr	Tr	Tr
Kaolinite	2	4	3	3
Illite/Mica	1	1	1	1
Illite/Smectite	1	Tr	Tr	Tr
Total	100	100	100	100

TABLE 5
Distribution of Resistivities in Drillholes on the East Flank of the Rock Springs Uplift near Corehole No. 2.

Drillhole number	Elevation of GWT, ft	Depth to GWT, ft	R_{us} 10 ft above GWT, Ω-m	R_s 10 ft below GWT Ω-m	Resistivity at 100 ft Ω-m	Resistivity at 200 ft Ω-m	Resistivity at 300 ft Ω-m
MSR-8	6,897	63	490	75	68	52	–
MSR-9	6,832	53	500	85	55	55	60
BD-1	6,703	232	v. high	38	650	650	–
BD-2	6,775	101	1,100	20	–	28	20
MSR-10	6,840	50	400	62	58	38	–
MSR-11	6,770	38	–	30	28	30	45
Corehole no. 2	*6,765*	*25*	*>100*	*28*	*35*	*60*	*30*
MSR-12	6,763	105	485	15	–	18	15
MSR-13	6,654	256	750	23	510	500	25
MSR-14	6,804	96	500	33	33	23	30
MSR-15	6,809	161	360	24	300	43	32
MSR-16	6,868	423	850	25	700	1,400	1,450

Explanations:

GWT - Ground water table
R_{us} - Resistivity measured in unsaturated zone
R_s - Resistivity measured in satured zone

All data except Corehole no. 2 interpreted from profiles in McClung et al. 1983

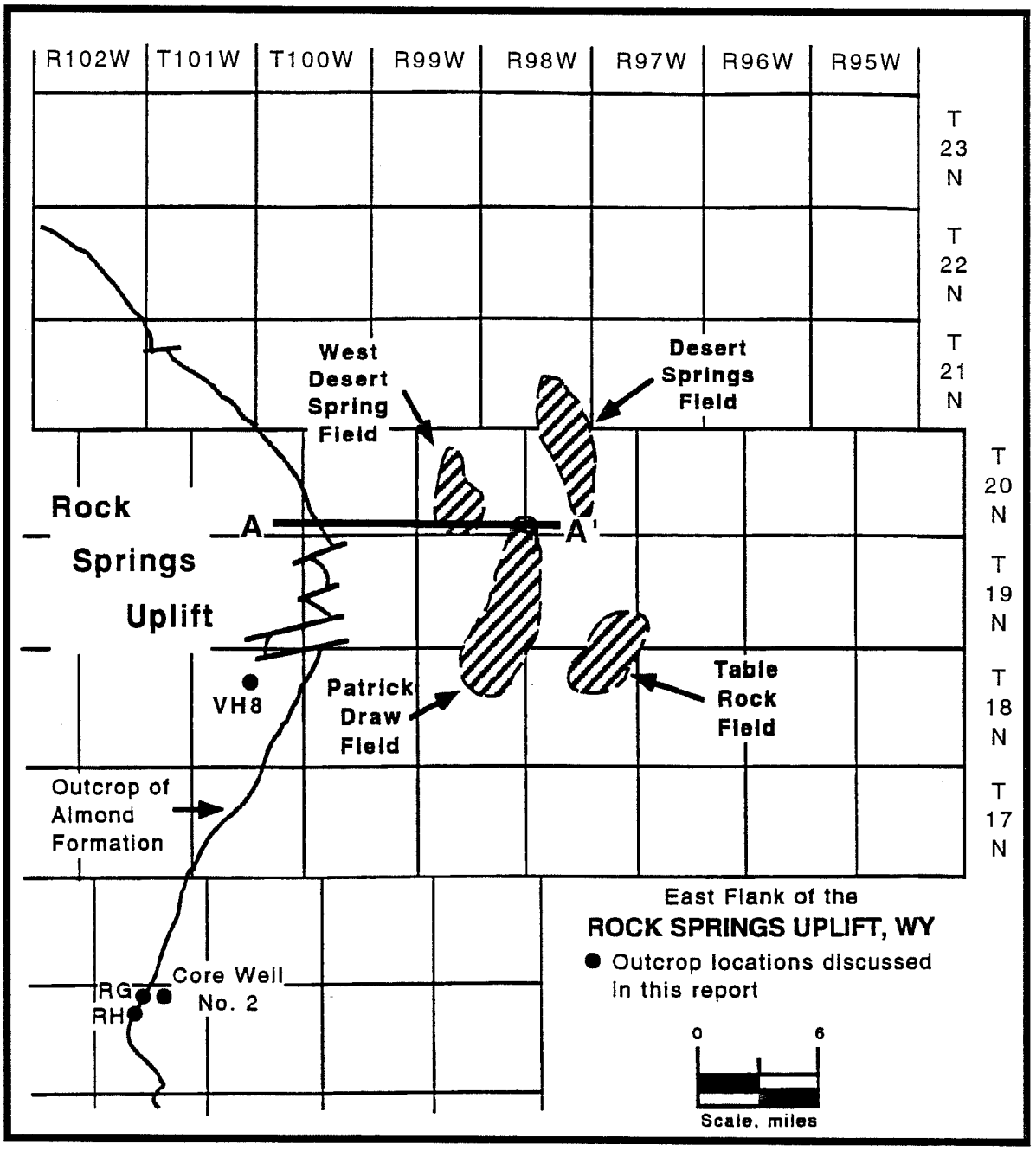

Figure 1. Location of Corehole no. 2, Almond Formation outcrop localities RG and RH, along the Rock Springs Uplift and fields producing from the Almond Formation

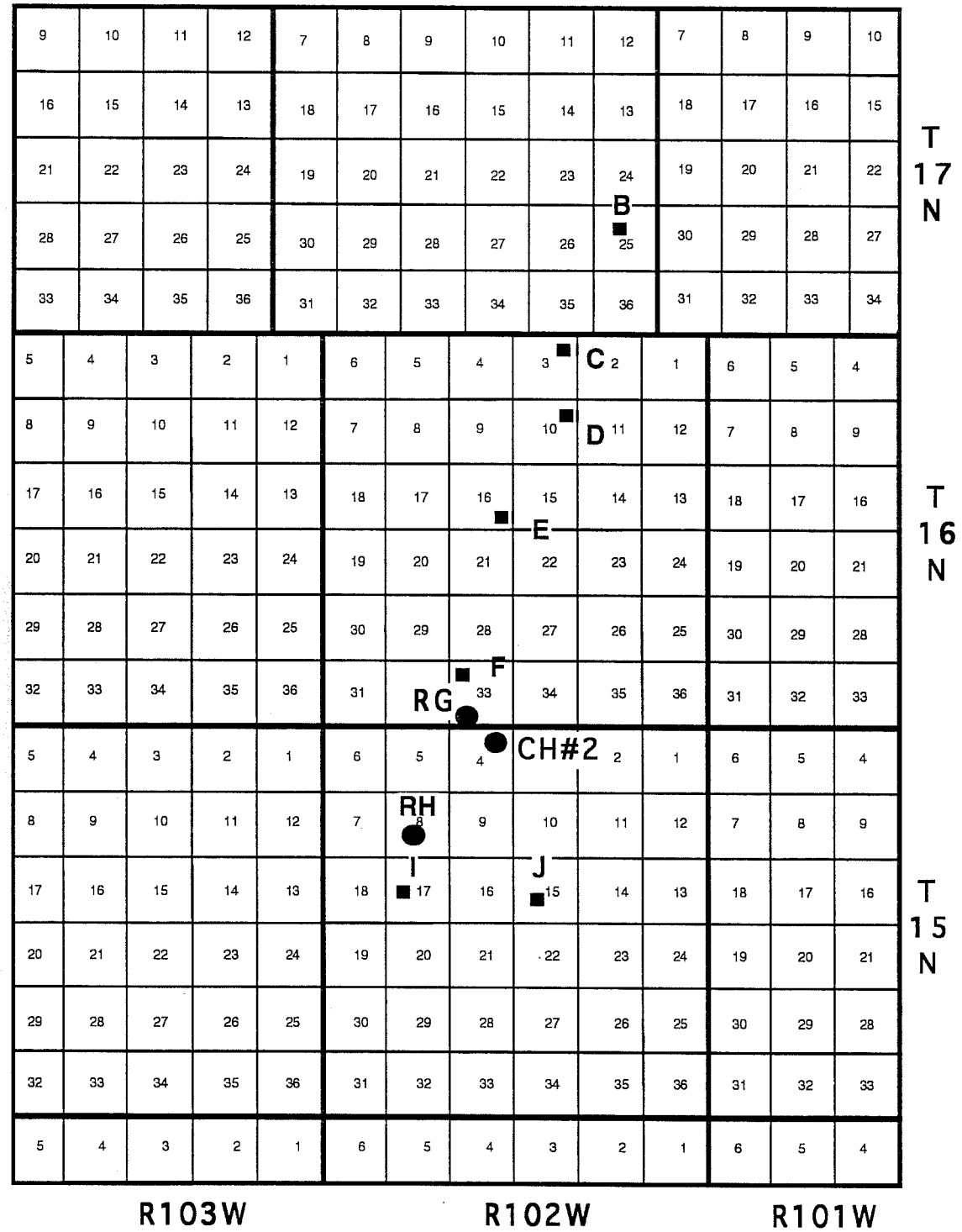

Figure 2. Location of Almond outcrops and Corehole no. 2 (CH#2) in Sweetwater Country, Wyoming indicated by circles. Other outcrops described in Roehler, 1988 are indicated by squares.

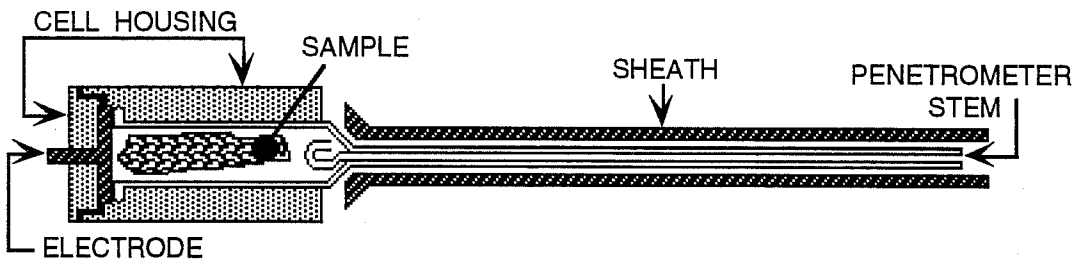

Figure 3. Penetrometer cross-section.

CORE HOLE NO. 2
NW NE NE Sec. 4 T15N R102W
Sweetwater County, WY
Mud Springs Ranch 7.5 Minute Quadrangle

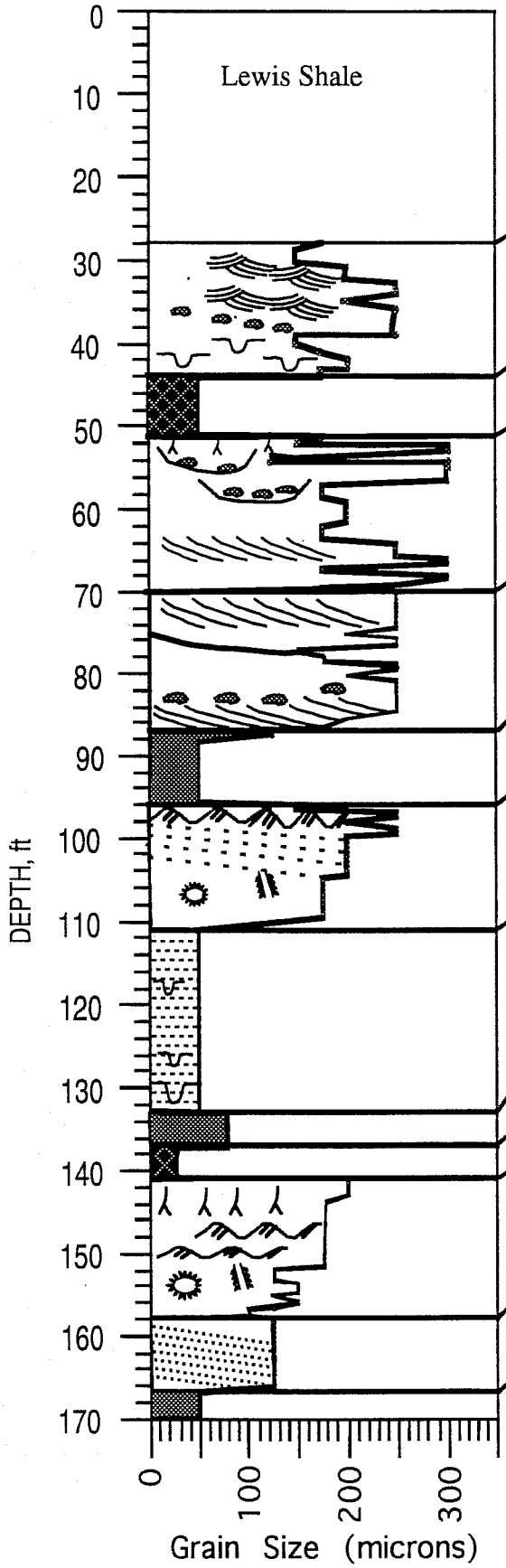

28-44' Sandstone (150-250 microns). Trough cross-bedding. Ripples along trough laminae at 33'. Rip up clay clasts and plant fragments at 37'. Burrowed to bioturbated 43-44'. Tidal Channel (80%).

44-50' Coal, Black and vitreous. Swamp (100%).

50-70' Sandstone (150-300 microns). Massive to faintly bedded, trough and medium angle planar bedded. Small scours with mudclasts at 54.2, 55.2, 55.4 and 58'. Laminae have alternating grainsize from 177 to 300 microns. Roots 50 to 50.5 ' Tidal Delta Ramp (80%)

70-87' Sandstone (250 microns). Faintly bedded, predominantly planar bedded with some medium to high angle bedding and a few possible troughs. High angle scour at 75 feet. Rip up clasts at 83 feet. Tidal Channel (80%).

87-96' Shaley Siltstone (30% shale). 1-inch thick beds of horizontally laminated siltstone. Shale is carbonaceous and ?pyritic. Bay or Lagoon (90%).

96-111' Sandstone (175-200 microns), 10% shale in burrows and dispersed. Faint laminations with alternating grain size between 177 and 250 microns indicate tidal influence. Ripples at 96'. 98-104' best sorted and least burrowed. Burrowing *Ophiomorpha*, 10%. Tidal Delta (75%)

111-133' Shale, Silty. Lenticular to wavy bedded. Horizontally laminated siltstone zones. Small coal lenses at 112.4 and 115.8'. Burrowing 60%, in discreet zones. More silty and burrowed at base. Bay or Lagoon (80%).

133-137' Siltstone, Sandy (sand size up to 177 microns) coaly fragments. Bioturbated. Lagoon (60%).

137-141' Coal. Swamp (100%).

141-158' Sand, (175 microns, alternating grain size 175-250 microns). Rooted at top of interval. Rippled to wavy bedded, small troughs at 155'. Burrowed 30% (*Ophiomorpha*) 156-157'. Tidal Delta (60%).

158-168' Sandstone, (125 microns). Faint low angle laminations. A few *Ophiomorpha* burrows. Splay (50%).

Figure 4a. Description and facies interpretations of Corehole no. 2. See Fig. 4c for legend.

CORE HOLE NO. 2
NW NE NE Sec. 4 T15N R102W
Sweetwater County, WY
Mud Springs Ranch 7.5 Minute Quadrangle

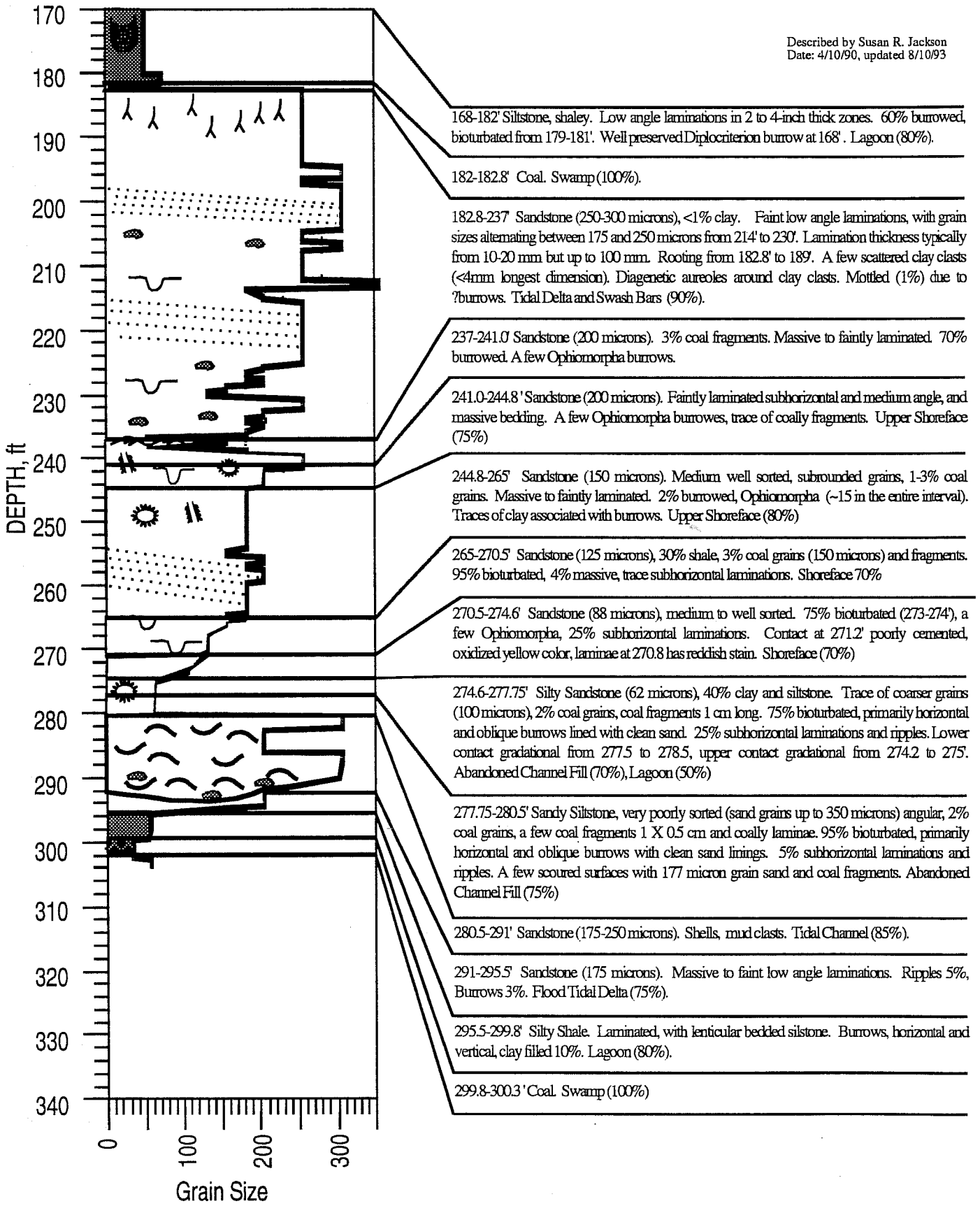

Figure 4b. Description and facies interpretations of Corehole no. 2 (continued)
See Fig. 4c for legend.

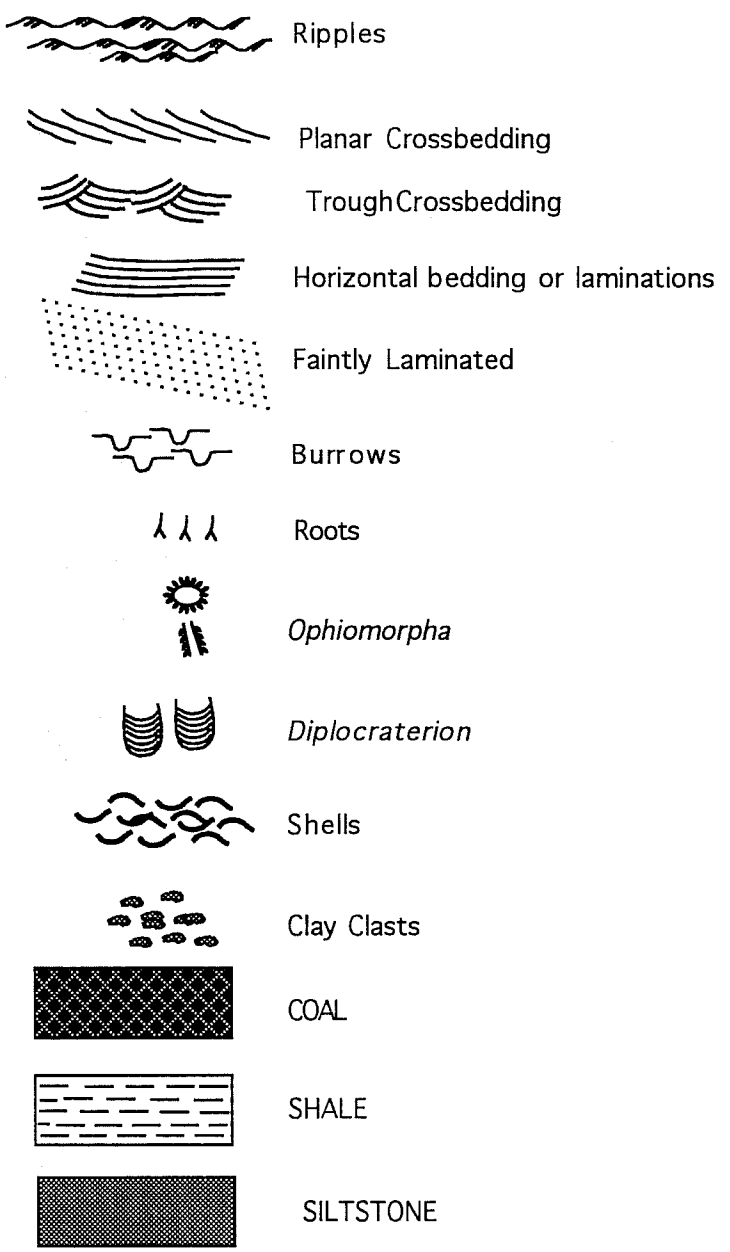

Figure 4c. Legend for measured section.

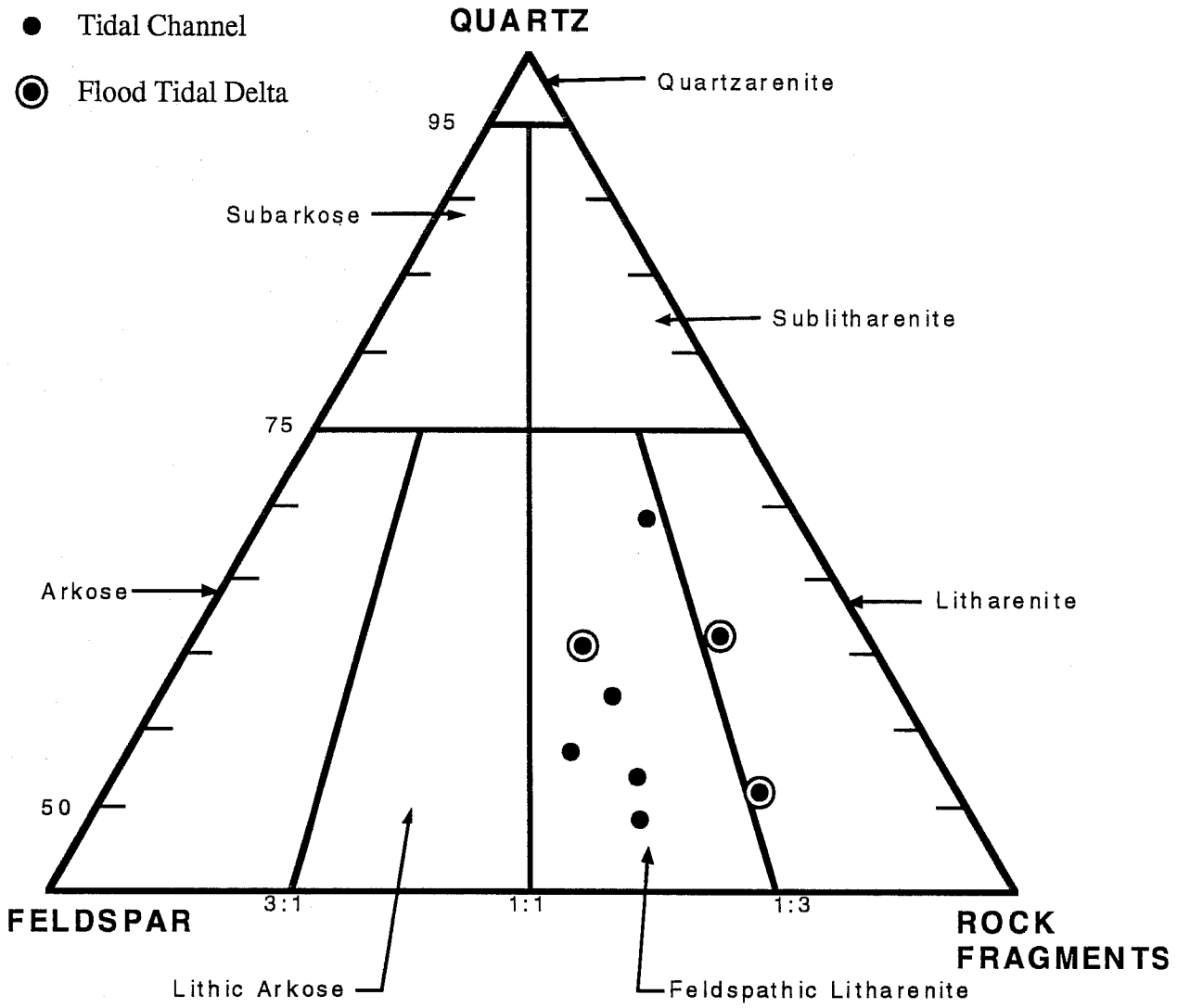

Figure 5. Trilinear Plot of quartz, feldspar, and rock fragment composition of the eight samples from Almond Corehole no. 2 that were analyzed petrographically.

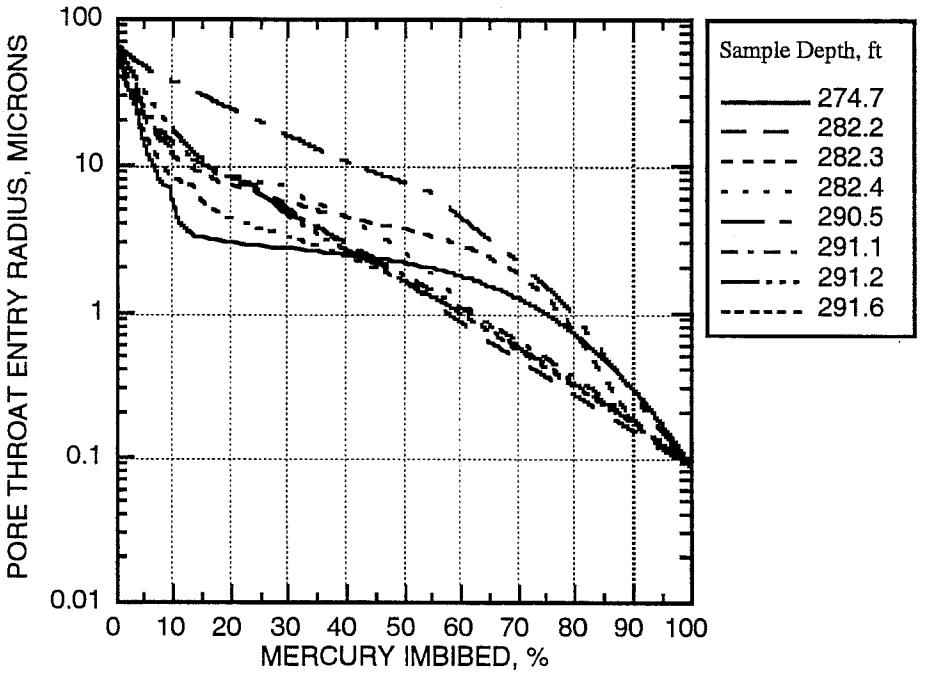

Figure 6.- Mercury injection-capillary pressure curves showing calculated pore-throat size distribution for eight samples from Almond Corehole no. 2. Note the overall similarity and fine pore throat radii for this family of curves.

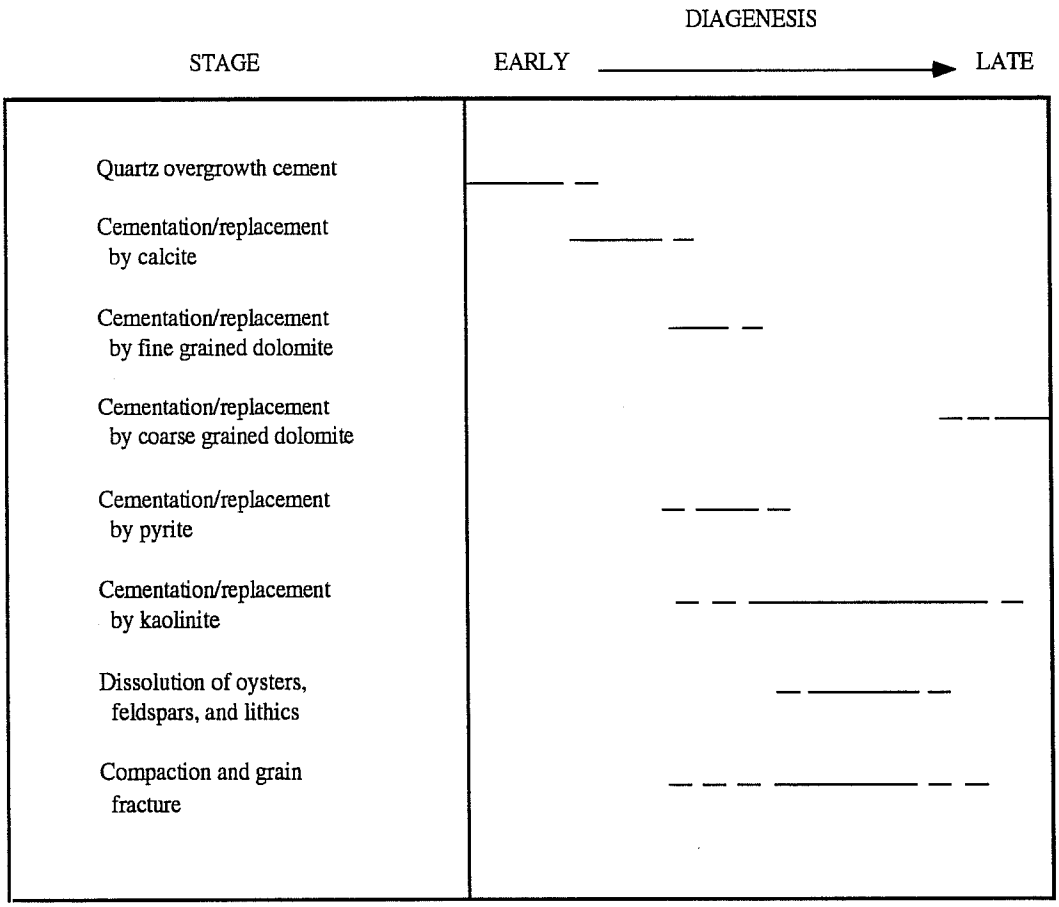

Figure 7- Diagenetic sequence proposed by analysis of eight sandstone thin sections from Almond Corehole no. 2 for the intrval 274-292 ft below surface.

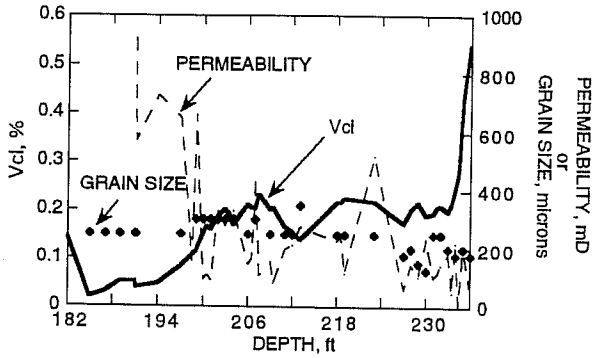

Figure 8a Distributions of clay content (V_{cl}), permeability and grain size in sandstone no.1

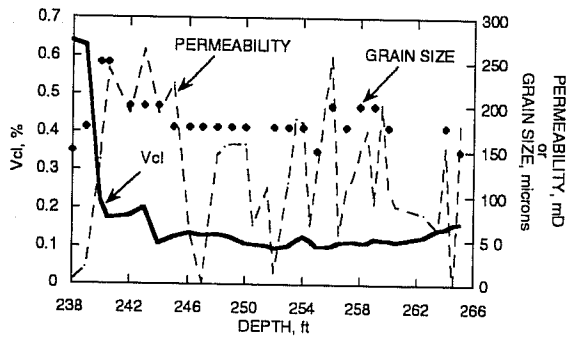

Figure 8b Distributions of clay content, permeability and grain size in sandstone no.2

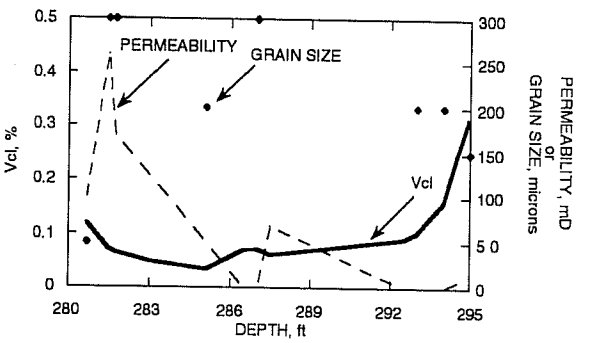

Figure 8c Distributions of clay content (V_{cl}), permeability and grain size in sandstone no.3

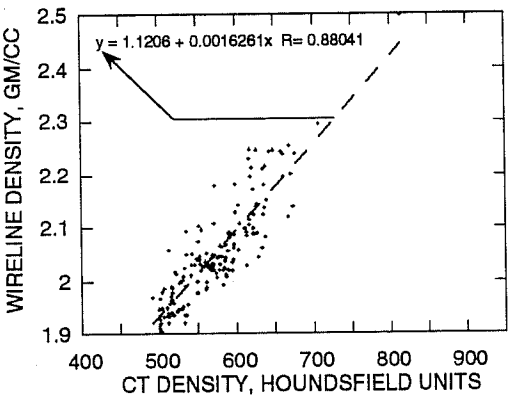

Figure 9. Cross plot of CT density and fluid corrected wireline log density in Corehole no. 2

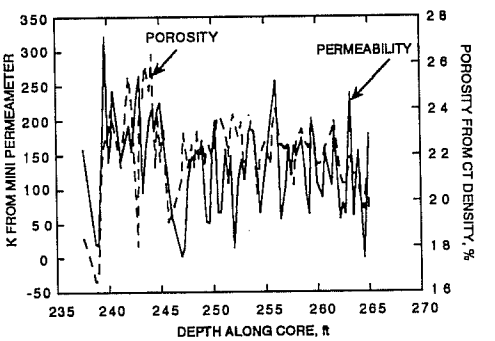

Figure 10 Distribution of porosity obtained from analysis of CT density and permeability from minipermeameter measurements in Corehole no. 2

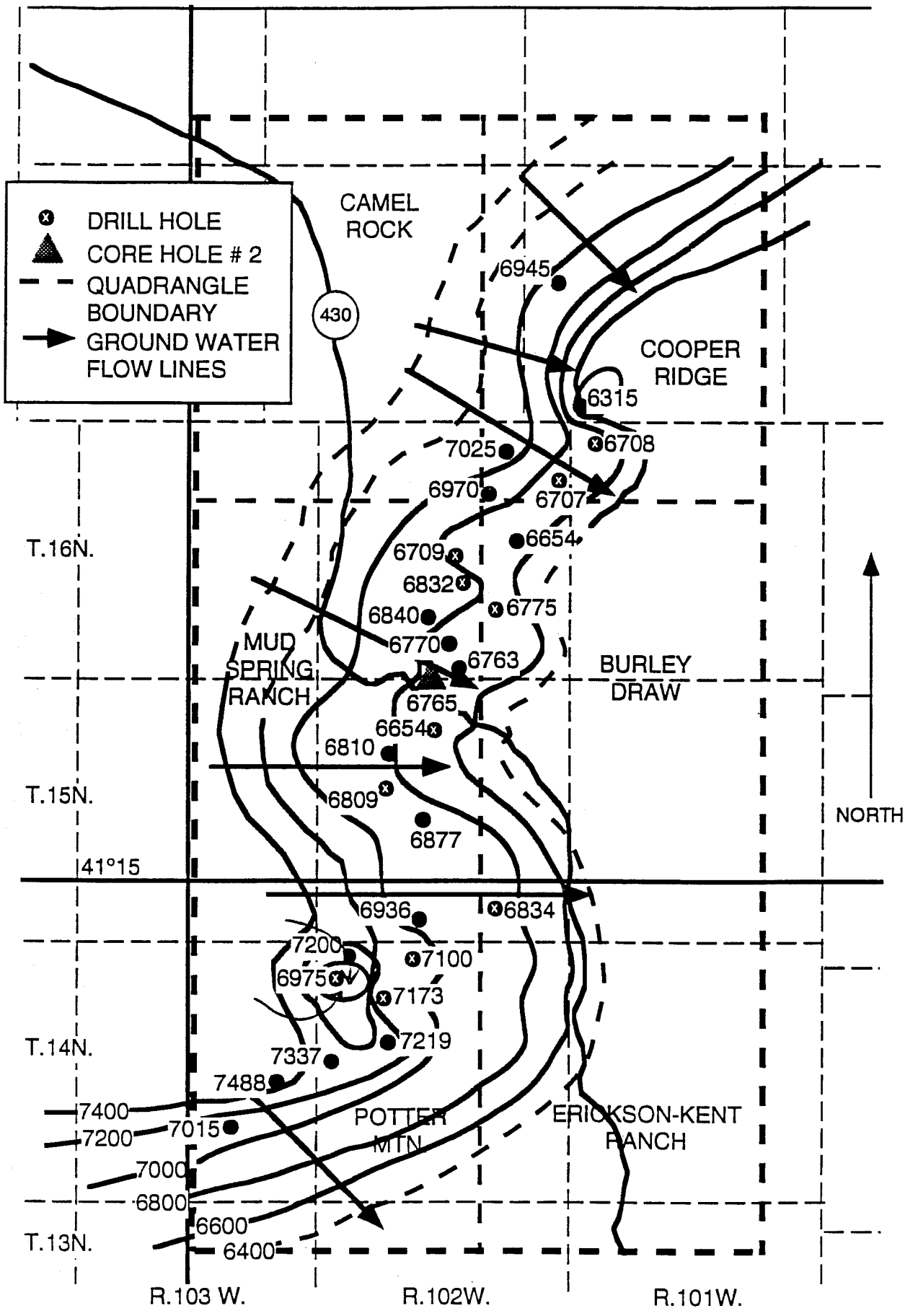

Figure 11. Ground water pressure head map in the area of Corehole no. 2 on the east flank of the Rock Spring Uplift. Potentiometric map shows the directions of ground water flow and defines the hydraulic gradients.